Deep-Sea Research Part II 162 (2019) 32–49

Contents lists available at ScienceDirect

Deep-Sea Research Part II

journal homepage: www.elsevier.com/locate/dsr2

Seasonal to mesoscale variability of water masses and atmospheric conditions in Barrow Canyon, Chukchi Sea

Robert S. Pickart[a,*], Carolina Nobre[a], Peigen Lin[a], Kevin R. Arrigo[b], Carin J. Ashjian[a], Catherine Berchok[c], Lee W. Cooper[d], Jacqueline M. Grebmeier[d], Ian Hartwell[e], Jianfeng He[f], Motoyo Itoh[g], Takashi Kikuchi[g], Shigeto Nishino[g], Svein Vagle[h]

[a] Woods Hole Oceanographic Institution, Woods Hole, MA, USA
[b] Department of Earth System Science, Stanford University, Stanford, CA, USA
[c] Pacific Marine Environmental Laboratory, Seattle, WA, USA
[d] University of Maryland Center for Environmental Science, Solomons, MD, USA
[e] National Oceanic and Atmospheric Administration, Silver Spring, MD, USA
[f] Polar Research Institute of China, Shanghai, China
[g] Japan Agency for Marine-Earth Science and Technology, Yokosuka, Kanagawa, Japan
[h] Institute of Ocean Sciences, Sidney, British Columbia, Canada

ARTICLE INFO

Keywords:
Barrow Canyon
Boundary currents
Wind-forced upwelling
Distributed Biological Observatory

ABSTRACT

Twenty-four repeat hydrographic transects occupied across Barrow Canyon from 2010 to 2013 are used to study the seasonal evolution of water masses in the canyon from July–October as well as the occurrence of upwelling. The mean sections revealed that the Alaskan coastal water is mainly confined to the eastern flank of the canyon, corresponding to a region of sloped isopycnals indicative of the surface-intensified Alaskan Coastal Current which advects the water. The Pacific-origin winter water is found at depth, banked against the western flank of the canyon. Its isopycnal structure is consistent with a bottom-intensified flow of this dense water mass out of the canyon. For the months that were sampled, the Alaskan coastal water is most prevalent in August and September, while the coldest winter water is observed in the month of August. It is argued that this newly ventilated winter water is delivered to the canyon via pathways on the central Chukchi Shelf, as opposed to the coastal pathway. Roughly a third of the hydrographic sections were preceded by significant up-canyon winds and hence were deemed to be under the influence of upwelling. During these periods, anomalously salty water is found throughout the eastern flank of the canyon, and, on occasion, Atlantic water fills the deepest part of the section. Using atmospheric reanalysis data, it is shown that upwelling occurs when the Beaufort High is strengthened and the Aleutian Low is deepened. Two modes of storm tracks were identified: northward progressing storms (mode 1) and eastward progressing storms (mode 2), both of which can drive upwelling. Mode 1 is prevalent in July–August, while mode 2 is more common in September–October. These seasonal patterns appear to be dictated by regional variations in blocking highs.

1. Introduction

Barrow Canyon is one of the primary conduits by which Pacific-origin water exits the Chukchi Sea into the Canada Basin. Based on data from a long-term mooring array at the mouth of the canyon, Itoh et al. (2013) calculated a mean northward transport of Pacific water of 0.44 Sv, which is approximately 50% of the mean transport through Bering Strait over the same time period (calculated using data from Woodgate et al., 2015). In the summer season this percentage seems to be even larger. Several recent observational studies have estimated that up to 1 Sv of Pacific water flows northward through the canyon during the summer months (Itoh et al., 2015; Gong and Pickart, 2015; Pickart et al., 2016).

The water approaches the canyon primarily via three main flow pathways on the Chukchi Shelf (Fig. 1). The coastal pathway, which in summertime is known as the Alaskan Coastal Current (ACC), provides the fastest and most direct route for water to travel from Bering Strait to Barrow Canyon (Weingartner et al., 1998). The other pathways are more circuitous and feed the canyon more slowly (Winsor and Chapman, 2004; Spall, 2007). In particular, the Central Channel

* Corresponding author.
E-mail address: rpickart@whoi.edu (R.S. Pickart).

https://doi.org/10.1016/j.dsr2.2019.02.003

Available online 11 February 2019
0967-0645/

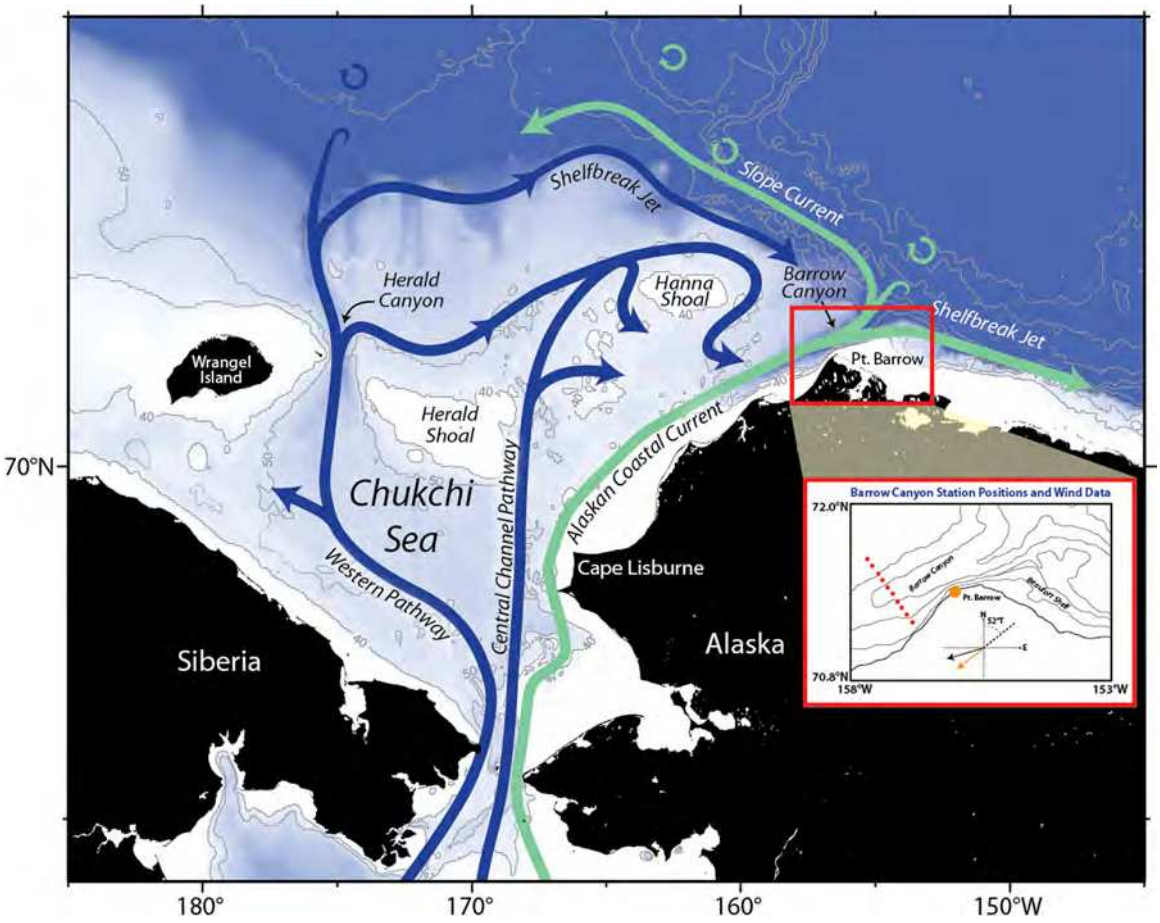

Fig. 1. Map of the study area and place names. The pathways of Pacific-origin water on the Chukchi Shelf, including the outflow from Barrow Canyon, is shown schematically (from Corlett and Pickart, 2017). The inset shows an enlarged view of Barrow Canyon. The nominal Distributed Biological Observatory (DBO) line 5 station positions are shown by the red circles, and the Barrow, Alaska weather station is the orange circle. The grey arrow represents a typical 10-m wind vector, where the orange component is the along-canyon value considered in the analysis (see text). (For interpretation of the references to color in this figure legend, the reader is referred to the web version of this article.)

pathway divides into filaments in the vicinity of Hanna Shoal (Weingartner et al., 2013; Pickart et al., 2016, Fig. 1), and, presumably, each of these filaments drains into Barrow Canyon. In addition, some of the water in the western pathway is diverted eastward and joins the Central Channel branch (Weingartner et al., 2005; Spall, 2007; Pickart et al., 2010). The timing by which the Pacific water in these interior shelf pathways is delivered to the canyon is presently unknown, although it is clear that this is strongly influenced by the wind (Winsor and Chapman, 2004).

The characteristics of the water masses that flow across the Chukchi Shelf vary markedly with season. In winter and early spring most of the shelf is filled with cold water near the freezing point (Pacini et al., 2016), which is referred to as newly ventilated Pacific winter water (NVPWW).[1] The water originates from the Bering Sea (Muench et al., 1988) and flows through Bering Strait, but it is also formed and/or further modified on the Chukchi Shelf (Weingartner et al., 1998; Itoh et al., 2012; Pacini et al., 2016). Later in the spring, warmer and fresher water flows through Bering Strait from the central Bering Shelf and the Gulf of Anadyr; north of the strait this mixture is referred to as Bering summer water (BSW,[2] e.g. Pisareva et al., 2015). During summer and early-fall, Alaskan coastal water (ACW) flows northward on the eastern side of Bering Strait. This is the warmest and freshest water that enters the Chukchi Sea, and it flows towards Barrow Canyon in the ACC. (At times the ACW can be fluxed westward onto the interior shelf due to wind-forced Ekman transport, even as far west as Herald Canyon, Pisareva et al., 2015). The final Pacific water mass found in the Chukchi Sea is referred to as remnant winter water (RWW, e.g. Brugler et al., 2014). This is winter water that has been warmed either by solar heating during the spring and summer or via mixing with Pacific summer waters. Of all of the Pacific water masses on the northeast Chukchi Shelf, the NVPWW has the highest nutrient content, which helps spur primary production (e.g. Hill and Cota, 2005; Lowry et al., 2015). While all of the water masses pass through Barrow Canyon at some point, their seasonal timing is presently unclear, as well as where geographically in the canyon they are found.

Ultimately the Pacific Water draining through Barrow Canyon enters the interior basin, but the manner by which this happens is directly influenced by the dynamics of the circulation in the canyon. As depicted schematically in Fig. 1, some of the Pacific Water exiting the canyon turns to the east and forms the Beaufort shelfbreak jet (e.g., Nikolopoulos et al., 2009). However, this accounts for only a fraction of the transport through Bering Strait. Recently it has been determined that a sizable portion of the Pacific Water flowing out of Barrow Canyon

[1] This water has been called various names, including winter-transformed Pacific Water (e.g. Pickart et al., 2005; Mathis et al., 2007), Pacific winter water (e.g. Spall et al., 2014; Pisareva et al., 2015), and newly ventilated Pacific winter water (e.g. Gong and Pickart, 2015; Pickart et al., 2016). We use the latter terminology here.

[2] BSW has also been called western Chukchi summer water (Shimada et al., 2001) and Chukchi summer water (von Appen and Pickart, 2012).

turns to the west and forms a current that progresses westward over the Chukchi continental slope. This has been named the Chukchi Slope Current, which has been determined to transport on the order of 0.5 Sv of Pacific water westward (Corlett and Pickart, 2017; Li et al., 2019). One must keep in mind, however, that the bifurcation of the flow emanating from Barrow Canyon into the eastward- and westward-directed currents depicted in Fig. 1 applies to the mean. It is well known that the circulation in the canyon varies on short timescales. For instance, the direction of the wind can strongly influence the flow, and, in particular, the behavior of the ACC (Shroyer and Pleuddemann, 2012; Okkonen et al., 2009). Eddies are also shed from the canyon (Pickart and Stossmeister, 2008), which is consistent with the vorticity structure of the canyon flow during certain times (D'Asaro, 1988; Pickart et al., 2005).

Perhaps the most common mesoscale process that occurs in Barrow Canyon is upwelling. It has been argued that a number of mechanisms drive such intermittent up-canyon flow. For example, using mooring data Aagaard and Roach (1990) argued that eastward-propagating shelf-edge waves can lead to upwelling. The modeling study of Signorini et al. (1997) suggested that time-varying outflow from the shelf can result in a rectified up-canyon flow at depth. Mountain et al. (1976) noted that large-scale changes in the meridional sea level gradient are a likely cause of upwelling. Another obvious candidate is wind. While Aagaard and Roach (1990) found no statistical correlation between the local wind and moored velocity records, there are documented instances of wind-driven upwelling in the canyon (e.g. Okkonen et al., 2009; Pickart et al., 2011, Pisareva et al., 2019). At times the upwelling is strong enough to advect Atlantic Water (AW) well onto the Chukchi Shelf (Bourke and Paquette, 1976). Recently, Ladd et al. (2016) documented multiple occurrences of AW as far south as Icy Cape, more than 200 km south of Barrow Canyon. Presently, however, it is not known what factors dictate the ability for AW to progress into (or beyond) the canyon, and what part of the canyon is in fact influenced by this warm and salty water.

As a main exit point of Pacific Water into the Canada Basin, and for Atlantic Water to intermittently flow onto the Chukchi Shelf, Barrow Canyon is an ideal place for studying and monitoring shelf-basin exchange. As mentioned above, long-term moorings have been in place at the mouth of the canyon (Itoh et al., 2013), and shorter-term mooring deployments have been carried out in the center of the canyon as well as at the head (e.g. Weingartner et al., 2017). While these timeseries have provided a wealth of information, the spatial coverage of moorings is limited both vertically and laterally. Starting in 2010, the Distributed Biological Observatory (DBO) program has facilitated the occupation of a repeat hydrographic transect across Barrow Canyon. This includes physical measurements as well as chemical and biological sampling. While the data collection is limited to the summer months, the transects provide a high-resolution view of the hydrographic structure of the canyon. This in turn offers the opportunity to assess the manner in which Pacific and Atlantic water are exchanged between the Chukchi Shelf and adjacent basin.

In this paper we use the first four years of repeat occupations of the DBO transect across Barrow Canyon to investigate the distribution of water masses in the canyon and how they vary over the summer and early fall. We also investigate wind-driven upwelling in the canyon and explore the atmospheric circulation leading to upwelling-favorable conditions. A main goal is to provide a full water column view of the hydrography of the canyon, which is impossible to obtain from moorings. The outline of the paper is as follows. We begin with a description of the DBO program and the shipboard hydrographic data, as well as the ancillary data used in the study. We then present the mean conditions in the canyon, followed by the seasonal progression of water masses from summer into fall. This is done both in the vertical plane and in temperature-salinity space. Lastly, we investigate the occurrence of upwelling in the canyon and elucidate the atmospheric conditions that drive this, including the patterns of storm tracks.

2. Data and methods

2.1. Shipboard hydrographic data

The primary source of data used in this study are hydrographic transects that were occupied as part of the DBO program. The concept behind DBO is that, as international ships of opportunity transit the Bering and Chukchi Seas doing their respective programs, they occupy one or more DBO lines as time permits. Five locations have been identified as biologically active areas, or “hotspots”, ranging from near St. Lawrence Island in the northern Bering Sea to Barrow Canyon in the northeast Chukchi Sea. Each ship participating in the program occupies a hydrographic transect at one or more of the identified sites, and, to the extent practical, measures a suite of biological and chemical variables – including sampling of the benthos. The objective is to construct timeseries at each site that help to elucidate regional differences in the ecosystem and how this is changing as the climate warms. The pilot phase of DBO began in 2010 (Grebmeier et al., 2010), and since then ships from six different nations have been occupying the sites on a regular basis.

For the present study we use the hydrographic occupations of DBO5, the transect spanning the central portion of Barrow Canyon (see the inset to Fig. 1). This section is comprised of 10 nominal stations at 5 km horizontal spacing. We use the 24 occupations obtained during 2010–13, which span from mid-summer to early-fall. As evidenced by the distribution of transects across years and months (Table 1), there were no strong seasonal or interannual biases in the sampling.

Each of the cruises used a Sea-Bird Electronics 911 + conductivity-temperature-depth (CTD) instrument with a SBE03 temperature sensor and SBE04 conductivity sensor. The sensors were sent to Sea-Bird for pre- and post-cruise calibration. On some of the cruises the conductivity sensors were also calibrated using bottle salinity data (deep water casts only). However, the DBO5 section is in relatively shallow water and the ranges in temperature and salinity on the Chukchi Shelf are quite large. As such, lack of an in-situ conductivity calibration does not impact the results of our study. All of the hydrographic data were collected and processed using Sea-Bird's software, ensuring consistency between the occupations. The downcast profiles were averaged into 1 db bins and any small scale noise removed.

We constructed vertical sections of the hydrographic variables for each of the transects. The variables considered were potential temperature referenced to the sea surface (hereafter referred to as temperature), salinity, and potential density referenced to the sea surface (referred to as density). A Laplacian-spline scheme was used to interpolate the data onto a standard grid with a vertical spacing of 5 m and horizontal spacing of 2 km. The grid extends from 0 to 50 km along the x axis (cross-canyon, where the positive direction is towards the Alaskan coast) and 0–130 m along the z axis (vertical). For the temperature-salinity diagrams, the original (non-gridded) data were used. The bottom topography for the standard section was constructed using soundspeed-corrected echosounder data from one of the cruises.

2.2. Atmospheric Reanalysis Fields

In order to investigate the large-scale meteorological context during the study period, we use the North American Regional Reanalysis fields (NARR, Mesinger et al., 2006). The space and time resolution of NARR is 32 km and 6 h, respectively. This product is an evolution of the original National Centers for Environmental Prediction (NCEP) global reanalysis and makes use of newer data assimilation and modeling advances that have been developed since then. The present study uses the NARR sea level pressure data and 10 m winds. Brugler (2013) validated the NARR data with the Barrow wind data described below.

Table 1
Occupations of the DBO5 transect used in the study.

Dates	Ship	Chief scientist
12 Jul 2010	USCGC Healy	Kevin Arrigo (Stanford University)
21 Jul 2010	CCGS Sir Wilfrid Laurier	Svein Vagle (Fisheries and Oceans Canada)
25 Jul 2010	R/V Xuelong	Jianfeng He (Polar Research Institute Of China)
24 Aug 2010	R/V Annika Marie	Carin Ashjian (Woods Hole Oceanographic Institution)
7 Sep 2010	USCGC Healy	Robert Pickart (Woods Hole Oceanographic Institution)
28 Sep 2010	R/V Mirai	Motoyo Itoh (Japan Agency for Marine-Earth Science and Technology)
20 Jul 2011	CCGS Sir Wilfrid Laurier	Svein Vagle (Fisheries and Oceans Canada)
22 Jul 2011	USCGC Healy	Kevin Arrigo (Stanford University)
29 Aug 2011	F/V Mystery Bay	Catherine Berchok (NOAA Alaska Fisheries Science Center)
1 Sept 2011	R/V Annika Marie	Carin Ashjian (Woods Hole Oceanographic Institution)
7 Oct 2011	USCGC Healy	Robert Pickart (Woods Hole Oceanographic Institution)
21 Aug 2012	NOAAS Fairweather	Ian Hartwell (NOAA)
22 Aug 2012	USCGC Healy	Jackie Grebmeier (University of Maryland Center for Environmental Science)
28 Aug 2012	F/V Aquila	Catherine Berchok (NOAA Alaska Fisheries Science Center)
24 Sept 2012	R/V Mirai	Takashi Kikuchi (Japan Agency for Marine-Earth Science and Technology)
10 Oct 2012	USCGC Healy	Robert Pickart (Woods Hole Oceanographic Institution)
23 Jul 2013	CCGS Sir Wilfrid Laurier	Svein Vagle (Fisheries and Oceans Canada)
8 Aug 2013	USCGC Healy	Lee Cooper (University of Maryland Center for Environmental Science)
14 Aug 2013	USCGC Healy	Lee Cooper (University of Maryland Center for Environmental Science)
24 Aug 2013	R/V Annika Marie	Carin Ashjian (Woods Hole Oceanographic Institution)
2 Sep 2013	R/V Aquila	Catherine Berchok (NOAA Alaska Fisheries Science Center)
3 Sep 2013	R/V Mirai	Shigeto Nishino (Japan Agency for Marine-Earth Science and Technology)
12 Oct 2013	USCGC Healy	Robert Pickart (Woods Hole Oceanographic Institution)
24 Oct 2013	USCGC Healy	Robert Pickart (Woods Hole Oceanographic Institution)

2.3. Meteorological timeseries

For the analysis of the upwelling we use wind data from the meteorological station located in Barrow, Alaska (recently renamed Utqiagvik). The data were acquired from the National Climate Data Center of the National Oceanic and Atmospheric Administration (NOAA) and subject to a set of quality assessment routines to remove erroneous values (see Pickart et al., 2013, for details).

2.4. Ice concentration data

For the ice concentration analysis, we used ice coverage percentage from the Advanced Very High Resolution Radiometer (AVHRR) and the Advanced Microwave Scanning Radiometer - Earth Observing System (AMSR-E), obtained from the National Climate Data Center (NODC) of the National Oceanic and Atmospheric Administration (NOAA). A blended product is available until September 2011, after which only AVHRR ice concentration data were used. The spatial resolution of the data is 0.25 degrees.

3. Results and discussion

3.1. Water mass analysis

3.1.1. Mean state

Using all 24 DBO5 occupations we created mean vertical sections of temperature, salinity, and density for the July-October period when the shipboard measurements were taken (Fig. 2). Using the satellite-derived ice data, we documented the ice concentration in the study region for each of the occupations. In every case there was open water in Barrow Canyon and in the surrounding area as well. The ice edge was typically far to the north of the transect.

To our knowledge, Fig. 2 represents the first mean view across Barrow Canyon that encompasses the entire water column. The warmest water in the section (>4 °C) is found above the eastern-most part of the canyon, which is due to the presence of ACW. The temperature front corresponding to the ACW is located near $x = 33$ km, where the 4 °C temperature contour outcrops and the 2 °C contour descends abruptly to deeper depths. Note that there is a density front here as well where the isopycnals start to slope downward progressing onshore. This is consistent with a surface-intensified ACC advecting this warm water northeastward out of the canyon; farther to the east the Beaufort shelfbreak jet is surface intensified when it transports ACW at this time of year (von Appen and Pickart, 2012). This thermal wind signature in the canyon indicates that the ACC extends to > 100 m and transports more than just ACW. The mean salinity section reveals that the ACW is not the freshest water found in the canyon. There is a layer of low-saline meltwater/runoff in the upper 20 m of the water column on the western side of the canyon (with values less than 30, discussed further below).

The coldest water in Barrow Canyon at this time of year is banked against the western side of the canyon, extending onto the interior shelf. It is perhaps surprising that this cold winter water is not found at the deepest part of the canyon, but this is likely due to a combination of factors. In their analysis of a synoptic survey of the canyon, Pickart et al. (2005) determined that NVWW sinks as it flows down the canyon; however, the canyon deepens rapidly to the north and the dense water finds an equilibrium depth well above the bottom due to the stratification. Another thing to note is that the densest winter water on the Chukchi Shelf is not always the coldest. Finally, warm AW was present at the bottom of the canyon in some of the occupations (see the upwelling analysis in Section 3.2). Although we do not have velocity information, we can infer that, in the mean, the winter water is being fluxed northward as a bottom-intensified flow. This is consistent with the fact that the isopycnals slope upward from the western side of the canyon towards the center (down to a depth of about 50 m). Our mean sections thus reveal that, during the summer months, ACW is advected northward on the eastern side of the canyon while winter water is transported northward on its western flank. We note that, farther to the north, some of the winter water transposes to the other side of the canyon (Pickart et al., 2005) and enters the Beaufort shelfbreak jet, while some of it remains on the western side and feeds the Chukchi Slope Current (Corlett and Pickart, 2017; Spall et al., 2018).

It is impossible to identify in the mean vertical sections precisely where all of the different water masses are situated, simply because, in the process of constructing the mean, they are averaged together to a

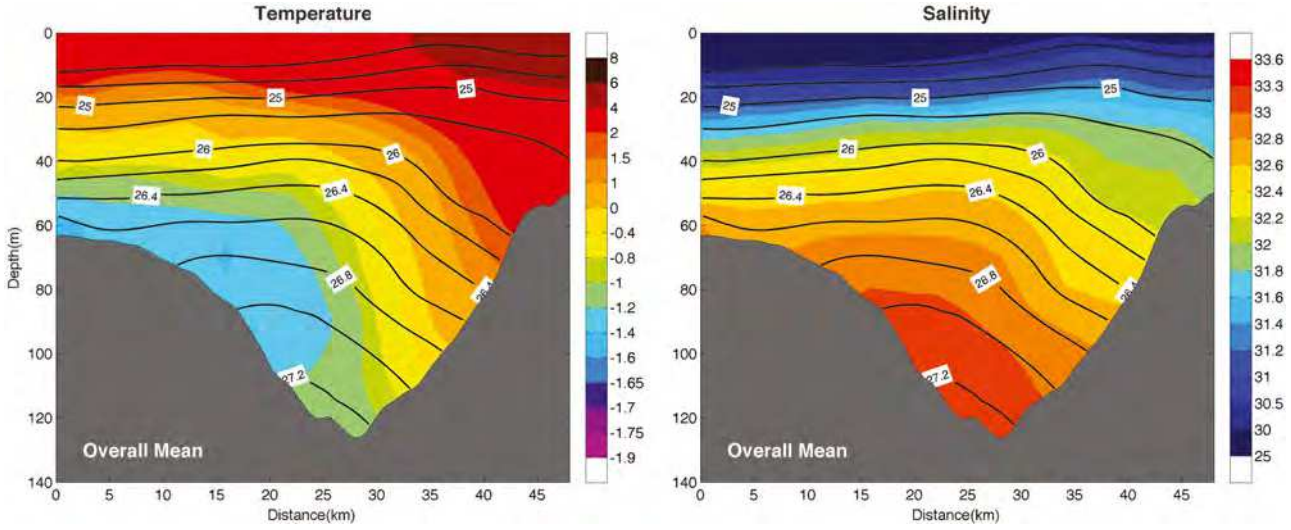

Fig. 2. Mean vertical sections of hydrographic properties from the 24 occupations of the DBO5 line. (a) Potential temperature (° C, color) overlain by potential density (kg m^{-3}, contours). The viewer is looking to the northeast. (b) Same as (a) except for salinity (color). (For interpretation of the references to color in this figure legend, the reader is referred to the web version of this article.)

certain degree. Hence, to investigate the presence of the various water types we computed a volumetric temperature-salinty (T/S) diagram (Fig. 3). In particular, we divided the T/S domain into bins and tabulated the number of realizations within each bin. The water mass boundaries in Fig. 3 are the same as those used in previous studies (e.g. Lin et al., 2016; Corlett and Pickart, 2017). We note, however, that these boundaries are not precise; for instance, there is interannual variability of the water properties flowing through Bering Strait (e.g. Pisareva et al., 2015). Nonetheless, the basic definitions used here are robust. As mentioned above, we consider four Pacific water masses: NVWW, RWW, BSW, and ACW, as well as AW and a near-surface water mass comprised of meltwater and runoff (the runoff includes snow melt, which could be an important contributor to the freshwater signal). We refer to this mixture as MW.

It is clear that winter water (i.e. NVWW and RWW) is the most common water type found in Barrow Canyon during the summer and early-fall (Fig. 3). Most of this falls within a narrow T/S range. NVWW has a very high nutrient concentration (e.g. Pickart et al., 2016), which is known to promote phytoplankton growth on the Chukchi Shelf and in Barrow Canyon (e.g. Hill et al., 2005; Lowry et al., 2015). The next most common water mass is BSW. As noted in the introduction, this is believed to be primarily a mixture between Anadyr Water and central Bering Shelf Water. However, as demonstrated by Gong and Pickart (2016), the densest and most weakly stratified type of BSW is in fact a modification of RWW. In particular, in early summer the RWW can be warmed either by solar heating within polynyas or by mixing with ACW along the ACC pathway, which converts the properties of the water to that of BSW. This is likely the reason for the large amount of BSW colder than 1 °C in Fig. 3. Note that there is another (smaller) peak in BSW between 2 and 3 °C that is fresher; the nature of this signal is explained in the next section.

While ACW is found in many of the DBO5 occupations, there is comparatively less of it than the other Pacific water masses. There are two “branches” of ACW in T/S space: a warmer, saltier branch and a colder/fresher branch. This is a seasonal effect which is discussed below. The two non-Pacific water masses found in the canyon are MW and AW. As seen in the mean vertical section of salinity, the former resides in the near-surface layer, while the latter appears intermittently near the base of the canyon (not evident in the mean vertical sections).

3.1.2. Seasonality in Temperature-Salinity space

There are clear trends in the water masses flowing through Barrow Canyon as the season progresses from July to October. This is demonstrated by constructing monthly versions of the volumetric T/S diagrams, which are shown in Fig. 4. Considering the winter water first, one sees that NVWW is only present in appreciable amounts during the month of August (see the insets). It is not immediately clear why this time range is so narrow. NVWW flows northward through Bering Strait through much of the winter and spring. Typically, the water in the strait is at or near the freezing point from January through April (Woodgate et al., 2005). Some of this NVWW water progresses into Barrow Canyon via the swift coastal pathway; data from the canyon indicate that it is present there in May and early-June (Codispoti et al., 2005; Weingartner et al., 2013; Pickart et al., 2016). However, the DBO data presented here, as well as other hydrographic data collected in June and July in the canyon (Gong and Pickart, 2015; Pickart et al., 2016), suggest that the last of the NVWW in the coastal jet has passed through the canyon before the end of June.

This begs the question, what is the source of NVWW present in Barrow Canyon in August and what dictates this timing? This is partially answered by considering the results of Pickart et al. (2016) who analyzed an extensive hydrographic/velocity survey of the northeast Chukchi Shelf in June-July 2011. They determined that the Central Channel pathway (with a contribution from the western pathway) bifurcates as it encounters Hanna Shoal, and, at this time of year, NVWW flows around both sides of the shoal towards Barrow Canyon. This is depicted schematically in Fig. 1 (for a detailed circulation map, see Fig. 9 of Pickart et al., 2016). It is also seen in the numerical model of Shroyer and Pickart (2019). In the 2011 shipboard survey of the shelf, the leading edge of the NVWW (which originated from Bering Strait) was located on the eastern side of Hanna Shoal in the middle of July, while the trailing edge was north of the Central Channel still a fair distance away from the shoal at the beginning of July. The average speed of the winter water was 10 km/day, and, based on the circulation diagram in Pickart et al. (2016), the distance from the leading edge to the center of Barrow Canyon (see the schematic of Fig. 1) is 300 km. This implies that the arrival time of the NVWW at the DBO5 line should be mid-August, which is consistent with the data presented here. Using similar reasoning, the trailing edge of the NVWW should pass through the canyon at the end of August / early September, again in line with our observations. Hence, it appears that the central shelf pathway delivers a second pulse of NVWW into Barrow Canyon during the August time frame.

Recall that the NVWW is associated with very high levels of

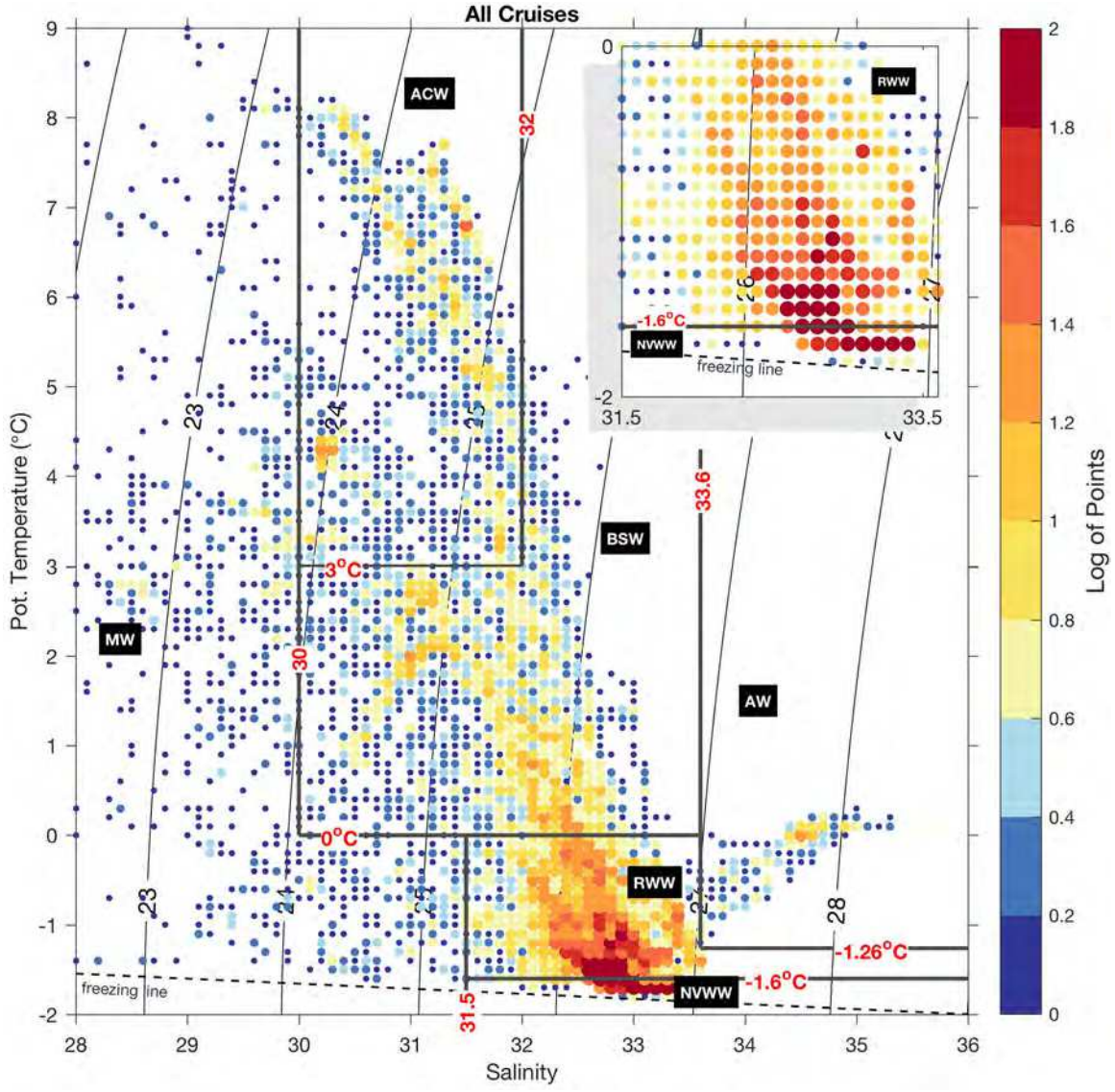

Fig. 3. Temperature-salinity diagram for all of the DBO5 occupations. The color corresponds to the frequency of occurrence of water within bins of 0.1 °C in temperature by 0.1 in salinity. The water mass boundaries are indicated by the grey lines. The inset shows an enlarged view of the winter water. The different water masses are: NVWW = newly ventilated winter water; RWW = remnant winter water; BSW = Bering Summer Water; ACW = Alaskan Coastal Water; MW = meltwater/runoff; and AW = Atlantic water. (For interpretation of the references to color in this figure legend, the reader is referred to the web version of this article.)

nutrients (e.g. Lowry et al., 2015; Pickart et al., 2016). This suggests that there is second period, later in the summer, when substantial amounts of nutrients are fluxed through Barrow Canyon into the basin. One might think, however, that drawdown along the relatively slow interior pathway would deplete the nutrients of the NVWW more so than in the swift coastal pathway of NVWW earlier in the season. This is difficult to assess because of the dearth of late-spring/early-summer nutrient data on the Chukchi Shelf. The Western Arctic Shelf-Basin Interactions (SBI) Program did measure the nitrate content of the NVWW in Barrow Canyon near the DBO5 line in late-spring 2002, which was in the range of $13-14\,\mu M/L$ near the bottom (Codispoti et al., 2005). By comparison, unpublished data from DBO5 occupations in 2010 show similar levels in the near-bottom layer of the canyon in late-summer (R. Pickart, pers. comm., 2011). While this constitutes limited evidence, it nonetheless suggests that drawdown does not deplete the nutrients in the near-bottom layer of NVWW in the central pathway, which is consistent with the shelf measurements presented in Pickart et al. (2016). This in turn suggests that both pulses of NVWW through Barrow Canyon – in late-spring and late-summer – deliver similar levels of nutrients to the basin. Additional measurements are needed to verify this.

Fig. 4 indicates that RWW is present in Barrow Canyon during each of the months, although it is found in greatest amounts in August and September. This makes sense in light of the above results. Recall that RWW is simply NVWW that has been warmed by solar heating and/or mixing with summer waters. September has the largest amounts of the densest variety of RWW, which is likely due to the moderation of some of the NVWW pulse circulating around Hanna Shoal.

BSW is also present during each of the months, but there are seasonal differences. In particular, there are large amounts of relatively dense BSW in July and August, which in part may be due to conversion of RWW to this water mass as noted above (and described in detail in Gong and Pickart, 2016). Note, however, that in October a separate peak of warmer and fresher BSW appears. This could be the result of cooling of ACW. One sees that the presence of the warm ACW is greatest in August and September, in line with the seasonal development of runoff and the ACC. In early fall, cold air and enhanced winds cool the ACW; indeed, the ACW signature has “collapsed” to colder

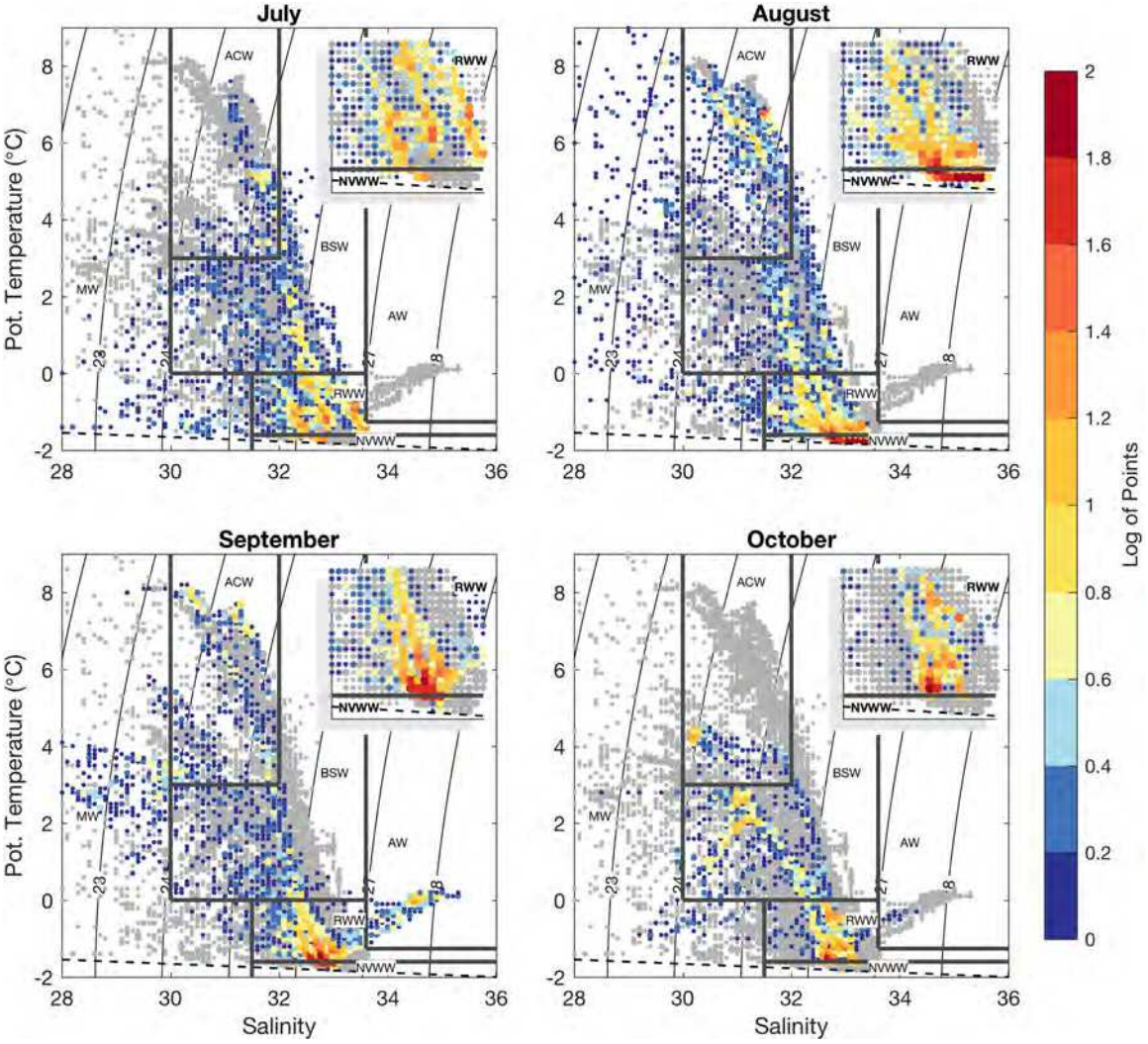

Fig. 4. Temperature-salinity diagrams for the months of (a) July, (b) August, (c) September, and (d) October. The color represents the frequency of occurrence as in Fig. 3. The insets show enlarged views of the winter water. The grey dots denote the data from all of the occupations. See the caption to Fig. 3 for the water mass names. (For interpretation of the references to color in this figure legend, the reader is referred to the web version of this article.)

temperatures in October (Fig. 4). Continued cooling would then transform this into the warm, fresh variety of BSW observed in October. Therefore, based on our data, it can be deduced that a significant amount of the BSW that flows through Barrow Canyon on its way to the interior basin is formed by local processes on the shelf. This is in contrast to the notion that this water mass is mainly a mixture of Anadyr water and Bering shelf water entering Bering Strait.

The character of the MW evolves from summer into fall as well. In July and August there are relatively large amounts of cold, salty water – i.e. early-season MW that is presumably influenced by mixing with winter water. In August into September, however, much warmer MW is present in the occupations. This is likely due to solar heating and a larger contribution from runoff (Cooper et al., 2016; Gonsior et al., 2017). Then in October the MW signature diminishes substantially, probably the result of mixing (the same process that modifies the ACW that month). Finally, our seasonal T/S plots reveal that most of the AW observed in Barrow Canyon was present during the month of September (none at all in July and August). This is addressed below in Section 3.2.

3.1.3. Seasonality in geographical space

We now investigate the seasonal presence of the different water masses in the vertical plane, which offers insights regarding the circulation in the canyon and the ultimate fate of the water. Using the water mass definitions in Fig. 3, we went through all of the synoptic occupations and determined where in the section each water type was located. This was then tabulated for each month as follows. For a given occupation, if a particular water mass was present, we shaded this part of the section a semi-transparent grey. These plots were then overlaid for each of the four months (Figs. 5–10). Hence, the darker the grey tone, the more realizations of that water mass during the month in question.

Consider first the ACW (Fig. 5). One sees that this water mass is generally found on the eastern side of the canyon above 60 m depth (consistent with the mean section of Fig. 2). Seasonally, it is more confined geographically (closest to the coast and shallowest) in July. It is most prevalent in August where there is a well-defined "wedge" inshore of $x = 35$ km. Then in September more ACW is found offshore, extending to the western end of the section; this is because of the upwelling favorable winds that month (see Section 3.2 below). Finally, in October only one of the transects measured ACW. The other warm Pacific water mass, BSW, shows less variation through the course of the four months (Fig. 6). As is the case with the ACW, this water mass is most prevalent on the eastern side of the canyon and sometimes occupies the same location in the water column as the ACW. It does, however, extend a bit deeper. Our data suggest that BSW flows out of the canyon more steadily than the ACW.

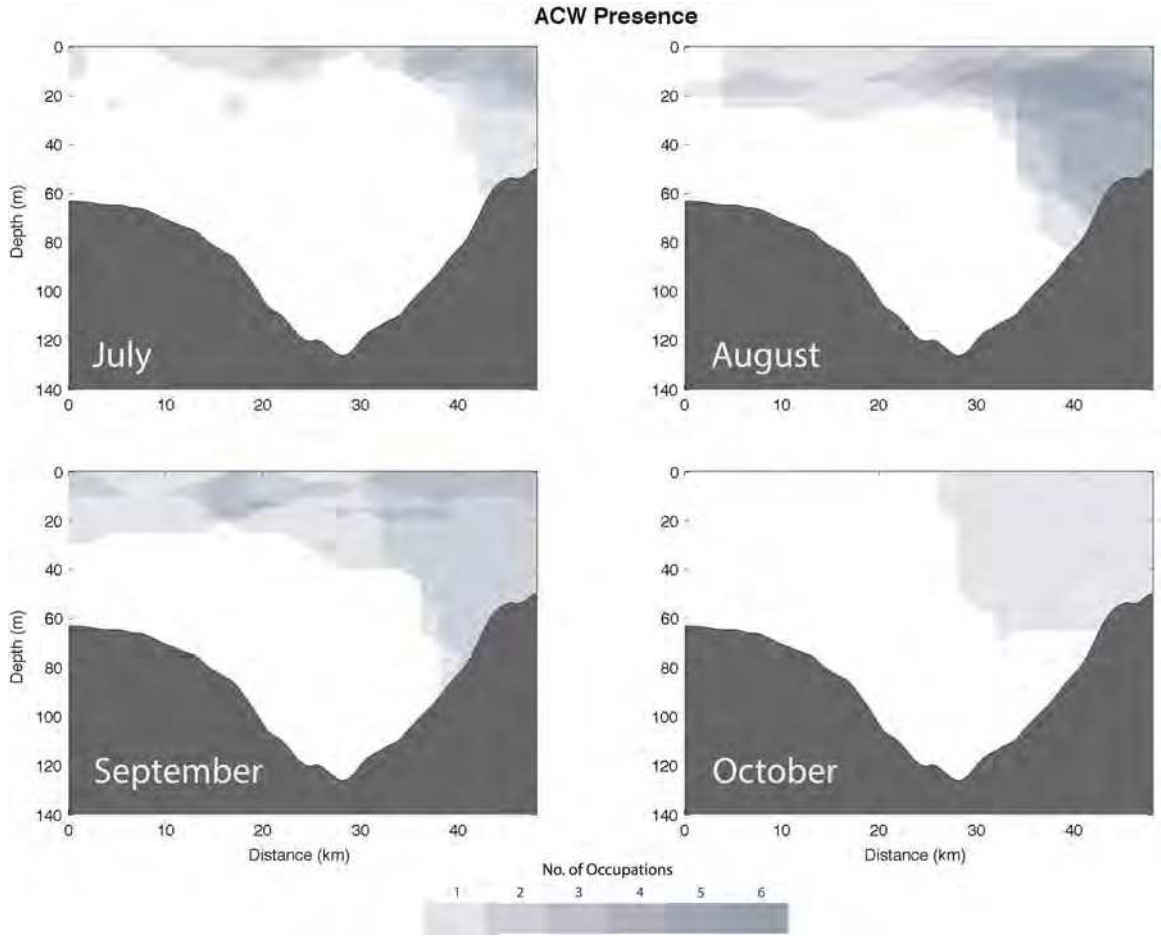

Fig. 5. Monthly presence of ACW. Grey shading marks where this water mass is present in each realization within the given month. The colorbar indicates the number of realizations. (For interpretation of the references to color in this figure legend, the reader is referred to the web version of this article.)

As noted above, NVWW mainly appears in the Canyon during the month of August. The vertical sections indicate that only a tiny amount of this water type is present in the other months (and none at all in October, Fig. 7). As was evident in the mean section, this water mass flows northward mainly banked against the western flank of the canyon. However there is synoptic variability in the position of the core, and at times it is found on the western edge of the canyon, while at other times it extends onto the base of the eastern flank. As explained above, the source of the NVWW in Barrow Canyon at this time of year is the central shelf. Based on a mass budget of the northeast Chukchi Sea, Pickart et al. (2016) deduced that the water flowing anti-cyclonically around the northern side of Hanna Shoal feeds the western side of Barrow Canyon. This is consistent with presence of NVWW observed in Fig. 7. By contrast, RWW is found in large amounts on both sides of the canyon (Fig. 8), although it is present more often on the western flank. There was a significant amount of RWW observed in each month, although a lesser quantity was found in October. Note that in August the RWW was more confined to the middle of the water column, in particular at the edges of the NVWW.

Early in the season (July and August), the majority of the MW is found on the offshore side of the canyon in the top 20 m (Fig. 9), although there is a small amount present in the ACC in August. Recall that during these months the MW is colder and saltier (see Fig. 4). It makes sense then that more of it is found offshore because the ACW tends to melt the ice in the ACC pathway earlier than this (Weingartner et al., 1998). In the latter two months, the warmer variety of MW (i.e. with an increased contribution due to runoff) is more evenly distributed across the canyon. Lastly, the AW is found near the bottom all along the eastern flank of the canyon (Fig. 10). As noted above it was observed predominantly in September, with a small amount present in October. This signature of AW arises because of wind-driven upwelling, which is described next.

3.2. Upwelling

As discussed in the introduction, upwelling occurs fairly regularly in Barrow Canyon, often driven by winds. We now consider those sections that were occupied under enhanced northeasterly winds in order to elucidate the hydrographic response within the canyon to such upwelling-favorable conditions.

First, it was necessary to characterize the winds in an objective manner. During an upwelling event, denser water from the basin is advected up the canyon, appearing near the deepest part of the DBO5 line and also along the eastern flank of the canyon. As such, we computed the average density anomaly over this region for each of the 24 occupations and compared this to the Barrow wind record. The highest correlation between the density anomaly and the wind record was for the component of wind along 52°T, which is approximately the axis of the canyon. This is not surprising, and is in agreement with the findings of Pisareva et al. (2019) who deduced the same angle using two years of wind and mooring data from the early 2000 s. Empirically, the clearest relationship between the wind and density anomaly occurred when we considered the wind over a three-day window prior to the mid-point time of the section. Those sections when the along-canyon wind speed exceeded 6.5 m s^{-1} for 20 h within this window were deemed upwelling realizations. We note that, while these are the optimal parameters, our

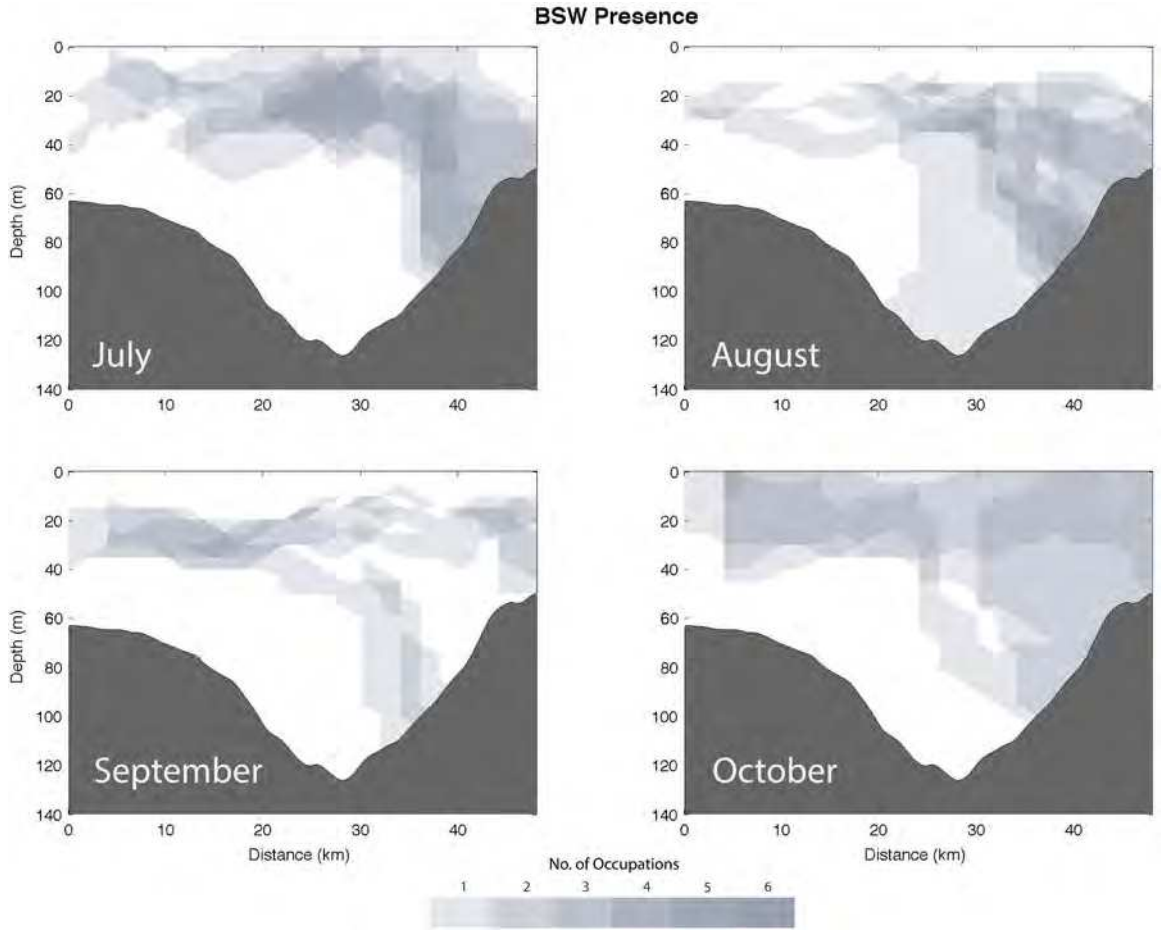

Fig. 6. Monthly presence of BSW. Grey shading marks where this water mass is present in each realization within the given month. The colorbar indicates the number of realizations. (For interpretation of the references to color in this figure legend, the reader is referred to the web version of this article.)

results are not sensitive to the precise values.

Based on the above criteria, 7 of the 24 sections were occupied during upwelling favorable conditions (Table 2): two in July, one in August, two in September, and two in October. In three cases AW was observed in the section (the only three such occupations out of the 24). The other upwelling realizations contained Pacific Water at the base of the canyon (see Table 2). It should not come as a surprise that upwelling was observed in each of the months and that not all of the cases involved AW. Using two years of mooring data on the Beaufort slope (roughly 150 km to the east of Barrow Canyon), Schulze and Pickart (2012) found that upwelling occurred throughout the year and that in only 25% of the cases was AW advected onto the shelf.

Notably, there was no obvious correlation between different wind metrics and the type of water upwelled (Table 2). This was the case when considering the peak wind speed over the time period that the wind exceeded 6.5 m s^{-1}, as well as the mean wind speed over this period. We also considered the number of hours of strongest winds, defined as the time during which the wind was greater than the e-folding value of the peak. Finally, we considered the product of the latter two quantities defined as C_{EK}, taken as a measure of the cumulative Ekman transport (Huyer et al., 1979; Pisareva et al., 2015). One might expect that AW would be advected into the canyon only during strong storms. However, Table 2 shows that AW was upwelled during storms with both large and small values of C_{EK}. Furthermore, RWW was upwelled for the storm with the second largest value of C_{EK}. One of the factors at play here is the type of water that resides offshore of the canyon at the onset of a given storm, which varies seasonally. As noted above, NVWW exits the canyon during the month of August (Fig. 7), and this water was found in the canyon during the August upwelling event (Table 2). Interestingly, in this realization the cold dense water was found on the eastern flank of the canyon (presumably flowing up-canyon), as opposed to the more typical scenario of residing on the western flank (flowing down-canyon). The reader is directed to Pisareva et al. (2019) for a more thorough investigation of the type of water upwelled in Barrow Canyon over the course of the full year. We also note the study by Lin et al. (2018) who showed that, in the Alaskan Beaufort Sea, upwelling of AW depends strongly on the wind stress curl over the continental slope, which dictates the offshore interface height between the Pacific Water and Atlantic Water.

In order to characterize the hydrographic structure of the canyon during upwelling, we composited the 7 upwelling transects and compared this to the composite of the 17 non-upwelling realizations (Fig. 11). The mean non-upwelling state shows the same basic features of the overall mean: the ACW resides above the eastern edge of the canyon while the winter water is banked on the western flank (compare Fig. 2 and Fig. 11a,b). However, the upwelled state is markedly different. The composite reveals that warmer, saltier water is present at the bottom of the canyon (Fig. 11c,d). While this salinity signal extends up the eastern flank, the same is not true for the temperature. This is made more clear by considering the anomaly sections (Fig. 11e,f). One sees that the salinity anomaly extends onto the eastern shelf and is in fact strongest at this shallow location. By contrast, while the temperatures are warmer at the bottom of the canyon, they become distinctly colder progressing up the eastern side of the canyon. As is true for salinity, the largest temperature anomaly is on the shelf. The likely explanation for this is that the Pacific Winter Water layer (be it NVWW or RWW) is advected up the canyon wall, displacing the BSW and ACW that normally reside there at this time of year (see Section 3.1.2), while

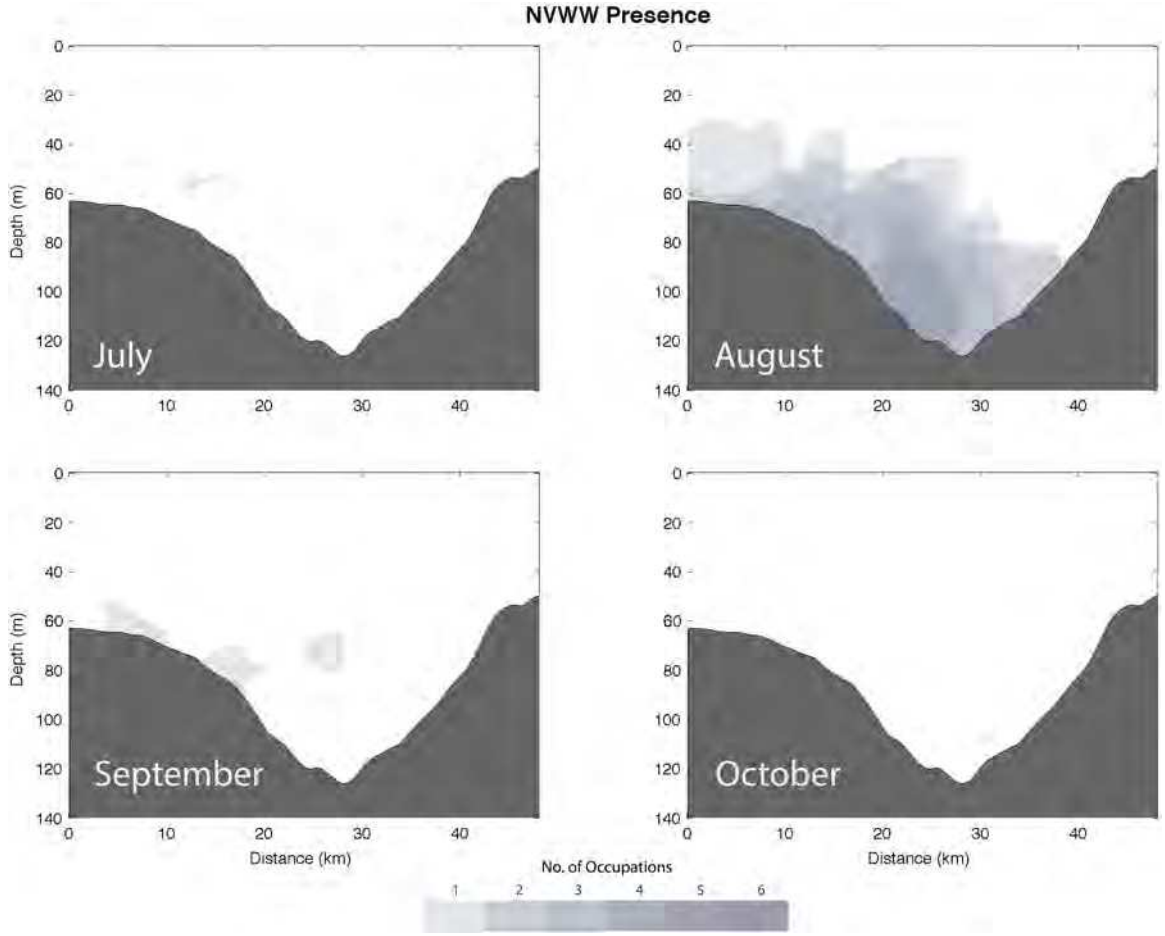

Fig. 7. Monthly presence of NVWW. Grey shading marks where this water mass is present in each realization within the given month. The colorbar indicates the number of realizations. (For interpretation of the references to color in this figure legend, the reader is referred to the web version of this article.)

the denser AW more readily influences the bottom of the canyon.

Another interesting hydrographic feature associated with the upwelling is the cooling of the surface layer across the entire transect, which is particularly evident in the temperature anomaly section (Fig. 11e). The reasons behind this are less clear. While Ekman transport should advect warm ACW offshore, wind mixing would tend to cool these waters. The hydrographic response of the surface layer also depends on the state of the ACC. Okkonen et al. (2009) found that, for northeasterly winds, the ACC is displaced offshore. However, for strong enough winds the current reverses to the south, (e.g., Danielson et al., 2017), although the storms considered here were not particularly powerful (Table 2). Clearly there are different factors at play, and the near-surface cooling observed here, as well as the cooling of the entire water column on the western edge of the canyon, merits further investigation (perhaps in a numerical framework).

Finally, it is worth documenting the upwelling response in T/S space (Fig. 12). While it is not meaningful to compare the frequency of water mass occurrences between the upwelling and non-upwelling states (there are far more realizations of the latter), the patterns show some clear differences. Most notably, the only time that AW was present in Barrow Canyon at the DBO5 transect was during wind-driven upwelling events. Conversely, ACW was only present outside of these times. It was noted earlier that, in October, a warmer variety of BSW appears at the DBO5 line which we argued was due to the conversion of ACW to BSW via atmospheric cooling. Fig. 12 reveals that this occurred during upwelling events. This suggests that wind-induced mixing can play an important role in the conversion of one Pacific water mass to another.

3.3. Atmospheric forcing

To examine the atmospheric conditions associated with upwelling, we used the Barrow wind data to identify all of the events that likely occurred during the months of July–October during 2010–2013 (i.e. not just the 7 cases when shipboard data were being collected in the canyon). In particular, we found all of the periods during which the up-canyon wind speed exceeded 6.5 m s^{-1}, where the length of the event was taken to be the time when the winds were stronger than the e-folding value of the peak wind (discounting any short dips below this threshold). Only events that were longer than 20 h were considered. Over the four-year study period there were 32 events totaling 190 days (versus 303 days of non-upwelling conditions).

Previous studies (e.g. Itoh et al., 2013; Pickart et al., 2013; Brugler et al., 2014) have demonstrated that the wind measured at Barrow is largely influenced by two atmospheric centers of action: the Beaufort High and the Aleutian Low. The former is a quasi-stationary region of high pressure located over the Beaufort Sea / Canada Basin, while the latter is the integrated signal of individual storms progressing from west to east along the North Pacific storm track. Using the NARR data, we averaged the sea level pressure (SLP) and 10 m wind fields for the upwelling and non-upwelling periods (Fig. 13). For the upwelling composite, the Beaufort High is well developed north of the Chukchi Sea, and there is a clear signature of the Aleutian Low centered over the eastern Bering Sea and Alaskan portion of North America (Fig. 13a). As a result, strong northeasterly winds are present throughout the Chukchi Sea, including Barrow Canyon, supported by the gradient in SLP between the two centers of action. By contrast, in the non-upwelling

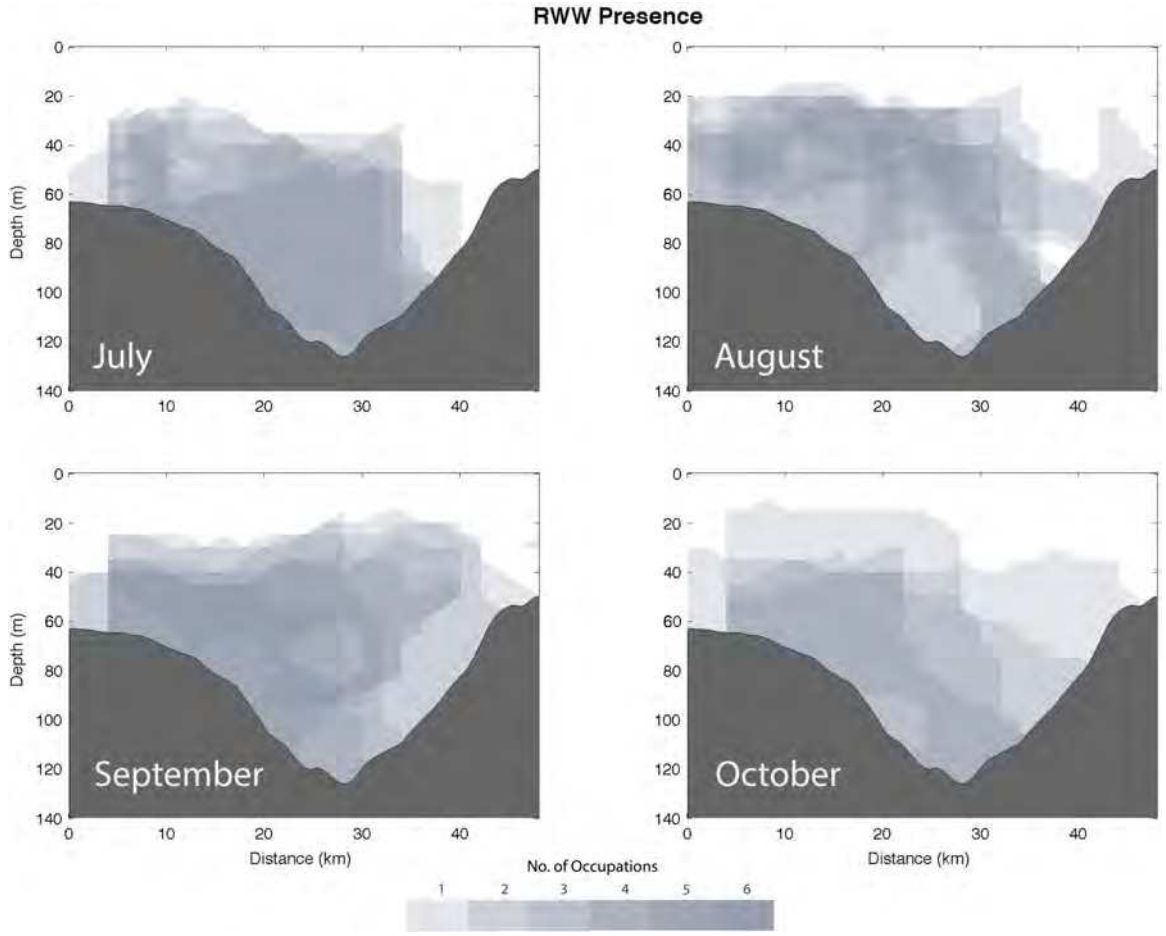

Fig. 8. Monthly presence of RWW. Grey shading marks where this water mass is present in each realization within the given month. The colorbar indicates the number of realizations. (For interpretation of the references to color in this figure legend, the reader is referred to the web version of this article.)

composite there is only a very weak signature of the Beaufort High and Aleutian Low (which are displaced to the east and west, respectively, Fig. 13b). In this case the winds are light in Barrow Canyon. These findings are consistent with Weingartner et al. (2017) who investigated aspects of upwelling in Barrow Canyon using mooring data.

In order to further understand the impact of atmospheric systems on the upwelling, we tracked the centers of all of the storms within the domain of Fig. 13 during the study period (July–October 2010–2013). The tracking was carried out visually using a graphical user interface (GUI) applied to the 6-hourly NARR fields. This technique has been used successfully in previous studies (e.g., VÅge et al., 2008; Pickart et al., 2009a). One of the main advantages of manual storm tracking, versus automated methods, is that there is little to no ambiguity regarding the merging and splitting of storms. Using data for fall/winter 2002–3, Pickart et al. (2009a, 2009b) showed that storms in this region that veer to the north and progress beyond roughly 65°N tend to cause upwelling in the Alaskan Beaufort Sea. This motivates us to consider if there are similar trends for the Barrow Canyon region during the summer and early-fall.

A total of 190 storms were identified for the study period. Of these, 174 entered the domain already formed, and 16 spun-up within the domain. Based on the calculated tracks, we divided the domain into a northern region (north of 62°N), a southwest region (west of 165°W), and a southeast region (east of 165°W). In Fig. 14 we show two dominant types of storm tracks: those that end up in the northern region (Fig. 14a), and those that end up in the southeast region (Fig. 14b). In the figure, the red asterisks denote where the storm was first identified in the study domain, and the blue lines are the tracks. Each segment of the tracks corresponds to the distance the storm traveled over the 6-h period. In the first scenario (Fig. 14a), the storms either entered the northern region from the west or progressed into that region from the southwest region. In the second case (Fig. 14b), the storms entered the southeast region either from farther south or progressed into that area from the southwest region. We refer to these two sets of storm tracks as mode 1 and mode 2, respectively. Together, the two modes account for roughly two-thirds of the storms. Overall, there were 64 mode 1 storms and 63 mode 2 storms. (The remaining 63 storms showed no discernible patterns.)

There is a clear seasonality associated with the two modes. Mode 1 storms are more frequent in summer and decrease in occurrence through the early fall (Fig. 15a). Conversely, mode 2 storms are less common in summer and occur more often in the later months. Using the Barrow timeseries we identified the storms that resulted in the 32 upwelling events. In many cases, multiple storms contributed to a given event. For example, as one storm weakened or moved out of the region, another storm would often strengthen or move closer and extend the event. In some instances up to 4–5 storms together resulted in a single upwelling event. (For each time NARR step only a single storm was identified as the dominant contributor, which was straightforward to discern.) In total, 85 storms influenced the 32 upwelling events: 27 storms were mode 1 and 32 storms were mode 2, which corresponds to 42% and 51%, respectively, of the two types of storms. The seasonality of occurrence of these two subsets is the same as for the full set of storms. Hence, mode 1 storms generally induce upwelling in summer, while mode 2 storms induce upwelling in early-fall.

To determine the canonical upwelling conditions for each mode, we

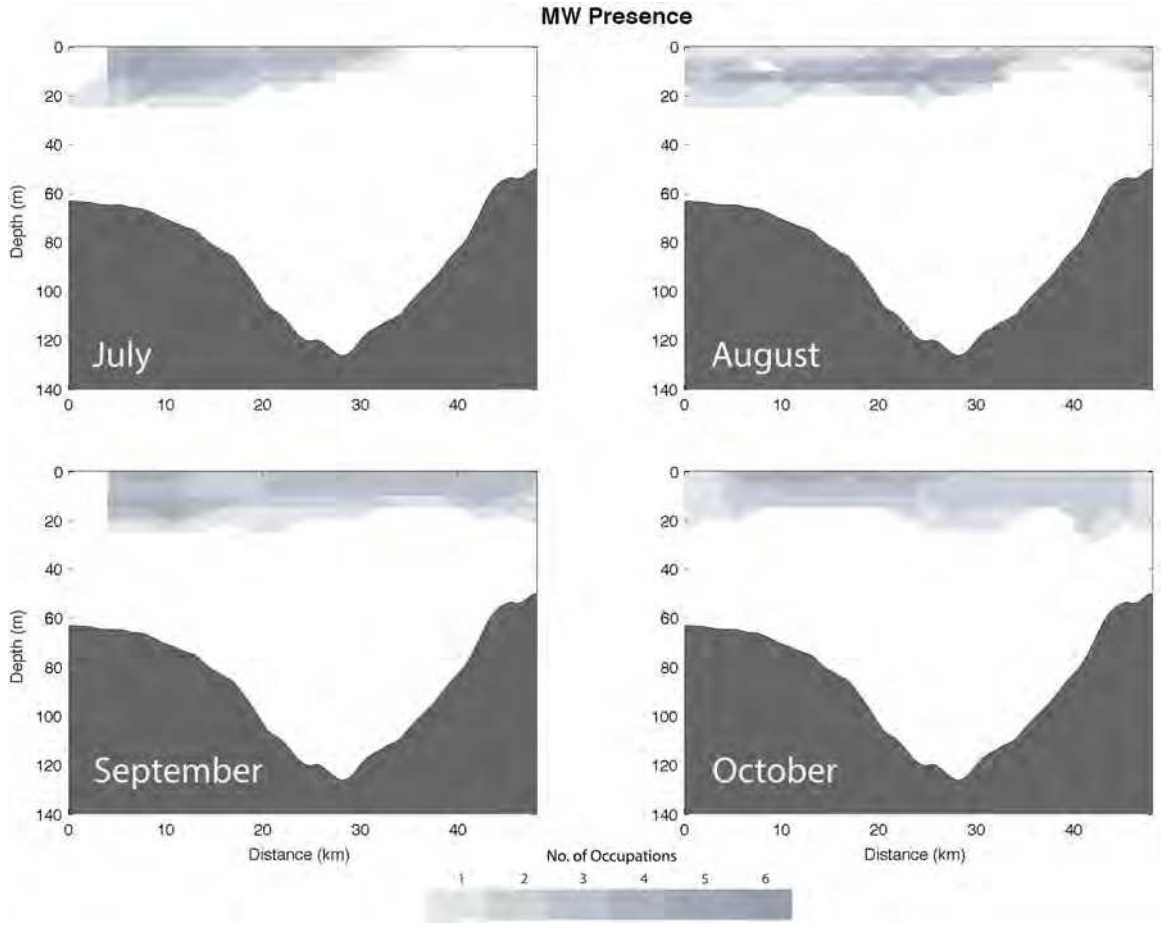

Fig. 9. Monthly presence of MW. Grey shading marks where this water mass is present in each realization within the given month. The colorbar indicates the number of realizations. (For interpretation of the references to color in this figure legend, the reader is referred to the web version of this article.)

composited the SLP and 10 m wind for the segments of tracks associated with enhanced winds in Barrow Canyon for the two cases. For mode 1, the composite reveals a well-developed Beaufort High and Aleutian Low, with the latter centered in the northeast Bering Sea (Fig. 16a). The analogous composite for mode 2 also shows a well-developed Beaufort High and Aleutian Low, except in this case both of the centers of action are stronger and the Aleutian Low is now centered more to the southeast near the Alaskan Peninsula.[3] In both instances the northeasterly winds in Barrow Canyon are comparable. The difference in the position of the Aleutian Low between the mode 1 and mode 2 composites is of course due to the difference in character of the storm tracks in mode 1 versus mode 2 (Fig. 14). We now consider the reasons behind the different modes.

In addition to the strong Beaufort High in the mode 2 composite (Fig. 16b), note the presence of high SLP in the southeastern part of the domain in the mode 1 composite (16a). We refer to this latter feature as the "southeastern high". Pickart et al. (2009a, 2009b) discussed the impact of high SLP blocking patterns in dictating the tracks of storms in their study of upwelling in the Beaufort Sea during fall/winter 2002–3. In light of that study, we considered the behavior of the Beaufort High and southeastern high in our data set by constructing climatological monthly mean values of SLP for these two regions over the full year. For the Beaufort High we used its year-long mean position (76.75°N, 147.75°W), and for the southeastern high we used the NARR grid point at the southeast corner of the domain (50°N, 130°W), which is where the SLP was generally a maximum. Results are not sensitive to these exact choices. In order to make the monthly means more robust we considered the time period 2000–2014. The resulting timeseries are shown in Fig. 15b. One sees that the magnitudes of the two regions of high SLP are out of phase. In particular, the southeastern high is strongest in summer, while the Beaufort High is weakest that time of year. Furthermore, during the four-month period considered in our study (July–October), there is a transition whereby the southeastern high dominates early in the period and the Beaufort High dominates later. This is in line with the variation in occurrence of the two storm track modes (Fig. 15a). The conclusion then is that a blocking southeastern high causes storms to veer northward (mode 1), while a blocking Beaufort High keeps the storms at a more southerly latitude (mode 2).

Recall that the seasonality in occurrence for the subset of storms that result in upwelling is similar to that for the entire set of storms shown in Fig. 15a. As such, we compared the composites of SLP and 10 m wind during times of upwelling in summer (July–August) and early-fall (September–October). The former is close to the composite for mode 1 upwelling storms (compare Fig. 16a and c), and the latter is similar to the composite for mode 2 upwelling storms (compare Fig. 16b and d). This strengthens our interpretation that upwelling is primarily induced by mode 1 storms in summer, when the southeastern high is intensified and acts as a block, in contrast to early fall when mode 2 storms cause upwelling, associated with a blocking Beaufort High.

4. Summary

This study used a collection of 24 hydrographic transects occupied

[3] The upwelling composite for the remaining storms (i.e. not mode 1 or 2) is similar to that of mode 1.

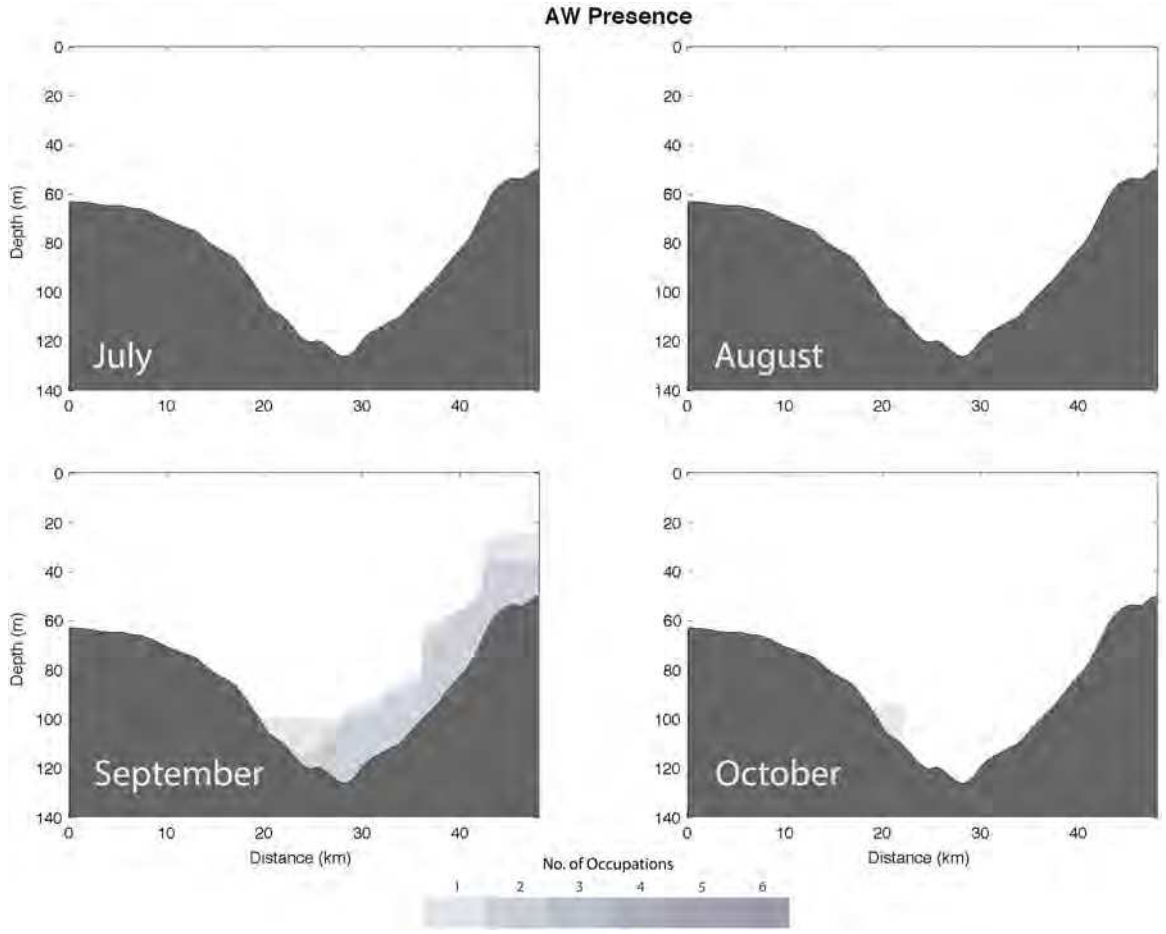

Fig. 10. Monthly presence of AW. Grey shading marks where this water mass is present in each realization within the given month. The colorbar indicates the number of realizations. (For interpretation of the references to color in this figure legend, the reader is referred to the web version of this article.).

across Barrow Canyon between 2010 and 2013 to study the seasonal evolution of water masses in the canyon from July–October as well as the occurrence of upwelling. The sections were carried out as part of the Distributed Biological Observatory (DBO) program, an international effort to obtain timeseries at key locations in the western Arctic. The mean summer/early-fall sections revealed that the Alaskan Coastal Water (ACW) is mainly confined to the eastern flank of the canyon, corresponding to a region of sloped isopycnals indicative of the surface-intensified Alaskan Coastal Current. The Pacific-origin winter water is found at depth, banked against the western flank of the canyon. The isopycnal structure in this region is consistent with a bottom-intensified flow of this dense water mass out of the canyon.

All of the Pacific-origin water masses were present in the canyon at some point during the four-month period. The most prominent water mass was the winter water, which is subdivided into very cold newly ventilated winter water (NVWW) and warmer remnant winter water (RWW). The NVWW appeared almost exclusively in August, which is consistent with earlier studies showing that this water mass is carried across the Chukchi Shelf via interior pathways. Our results suggest that these pathways deliver the dense winter water to Barrow Canyon within a month-long window in late summer. The next most prominent water mass was Bering Summer Water (BSW), which was measured during each month of the study period. The ACW had its maximum presence in August and September. Our analysis indicates that this water mass is converted to a relatively warm, fresh variety of BSW in October,

Roughly a third of the hydrographic sections were preceded by significant up-canyon winds and were categorized as under the influence of upwelling. The composite average of these cases, compared to the non-upwelling realizations, revealed that anomalously salty water is found throughout the eastern flank of the canyon during upwelling. At the base of the canyon the water is warmer than average, while near the

Table 2
Upwelling metrics for the transects occupied under enhanced up-canyon winds. See the text for details.

Date of section	Upwelled water mass	Peak wind speed ($m\ s^{-1}$)	Mean wind speed ($m\ s^{-1}$) ($\overline{u_w}$)	Strong wind hours (t_w)	$C_{EK} = \overline{u_w} \times t_w$
12 Jul 2010	RWW	11.9	7.6	22	167
21 Jul 2010	RWW	10.5	8.5	34	290
7 Oct 2011	RWW	9.4	7.6	28	213
24 Sep 2012	AW	10.2	8.2	11	90
3 Sep 2013	AW	14.2	11.4	27	307
8 Aug 2013	NVWW	11.8	8.3	22	182
12 Oct 2013	AW	12.2	9.1	15	136

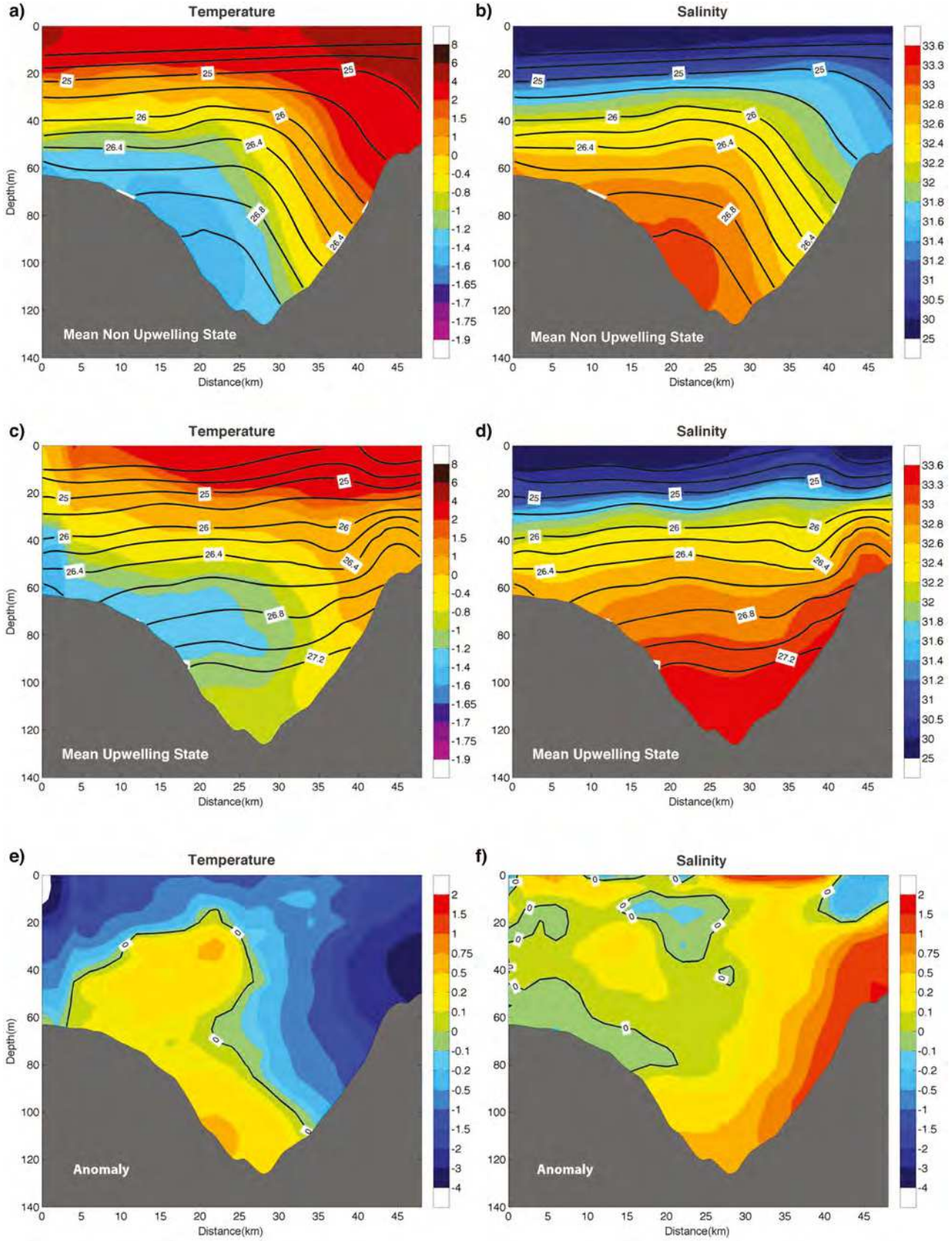

Fig. 11. Composite vertical sections of the upwelling realizations compared to the non-upwelling realizations. Top panel: non-upwelling mean. (a) potential temperature (° C, color) overlain by potential density (kg m^{-3}, contours); (b) salinity (color) overlain by potential density (contours). Middle panel: upwelling mean. (c) potential temperature (color) overlain by potential density (contours); (d) salinity (color) overlain by potential density (contours). Bottom panel: anomaly sections (upwelling minus non-upwelling). (e) potential temperature (° C); (f) salinity. The thick black line marks the zero contour. (For interpretation of the references to color in this figure legend, the reader is referred to the web version of this article.)

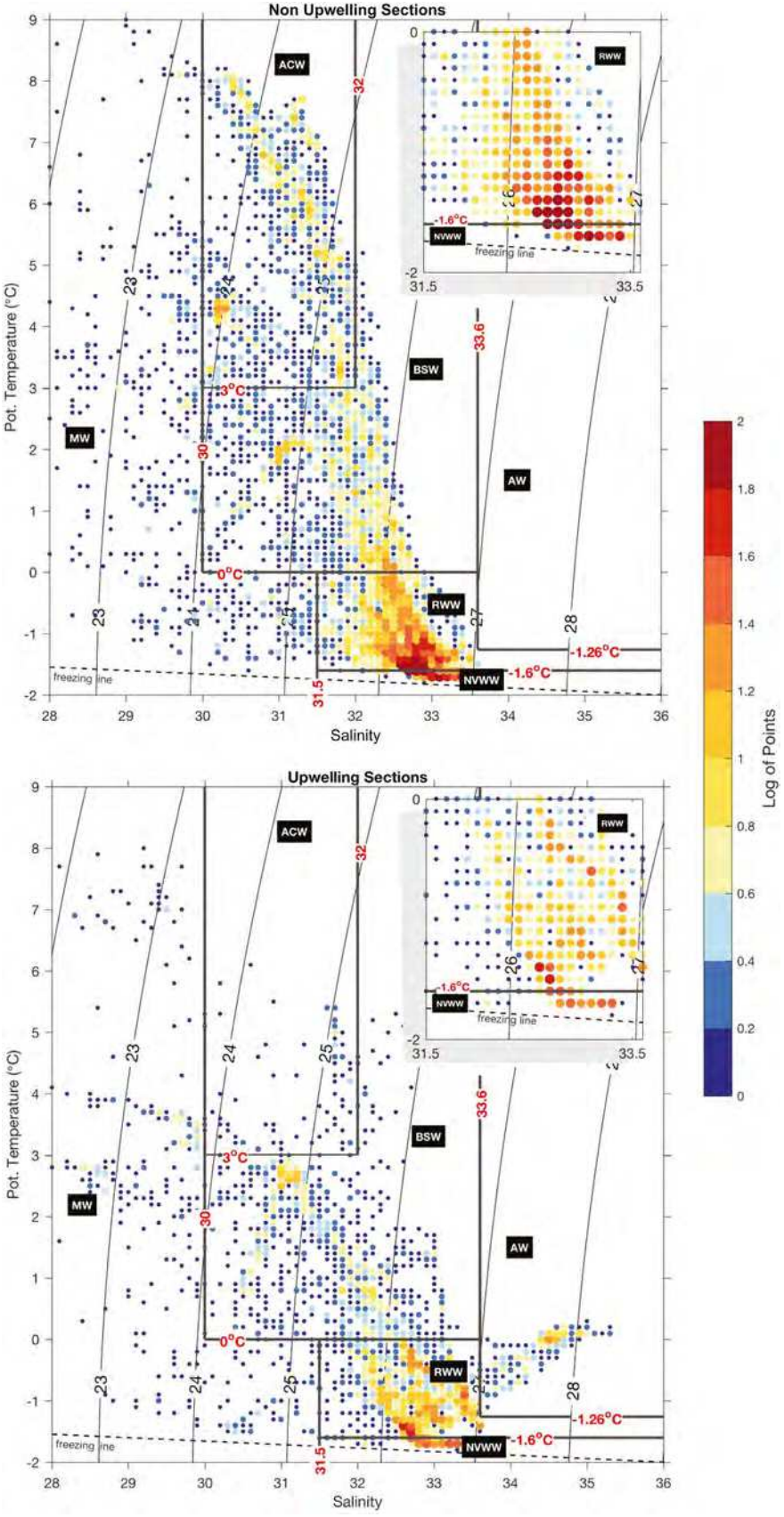

Fig. 12. Temperature-salinity diagrams for the (a) non-upwelling DBO5 transects and (b) upwelling transects. The color represents the frequency of occurrence as in Fig. 3. The insets show enlarged views of the winter water distribution. (For interpretation of the references to color in this figure legend, the reader is referred to the web version of this article.)

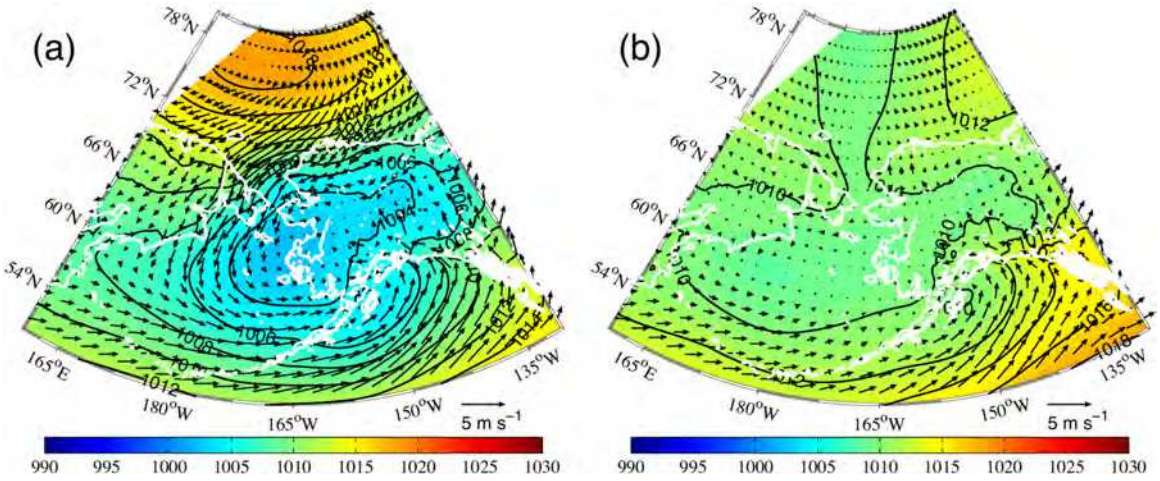

Fig. 13. Composites of sea level pressure (color, mb) and 10 m wind (vectors, m s^{-1}) from NARR for (a) upwelling, and (b) non-upwelling periods. (For interpretation of the references to color in this figure legend, the reader is referred to the web version of this article.)

shelfbreak the water is colder than average. This reflects the fact that warm, salty Atlantic Water (AW) is occasionally upwelled into the canyon, while the colder Pacific-origin winter waters that normally occupy the deepest part of the canyon are drawn to shallower depths. The only time that AW was measured in the canyon was during such wind events, at which time ACW was absent from the canyon. Our data indicate that the conversion of ACW to BSW occurs via wind mixing during the upwelling.

Using reanalysis fields we characterized the atmospheric circulation associated with upwelling in the canyon during the four-month study period. To get a larger sample size we used the Barrow wind data to identify likely upwelling events using a similar criteria as that applied to the hydrographic sections. Consistent with previous studies, we found that upwelling occurs in the canyon when there is an enhanced Beaufort High north of the Chukchi Sea and a deep Aleutian Low in the Bering Sea. To elucidate the nature of the atmospheric patterns, we tracked all of the storms in the domain during the study period, which revealed that there are two dominant modes: one in which the storms mainly progress to the north (mode 1), and the other when they predominantly progress to the east (mode 2). The mode 1 storms are more common in the summer, while the mode 2 storms occur more frequently in the early-fall. Both types result in upwelling roughly half the time. Our analysis suggests that the relative strength of the Beaufort High versus a region of high pressure in the southeast part of the domain (referred to as the southeastern high) dictate this seasonality. In particular, in July–August the southeastern high acts as a block which causes more storms to progress northward, while in September–October

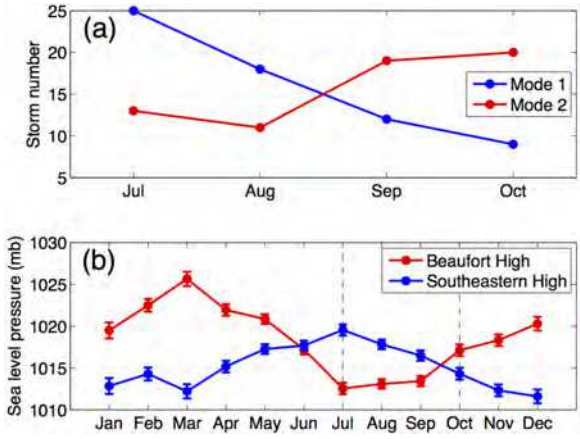

Fig. 15. (a) Monthly occurrence of the two storm track modes during the study period. (b) Climatological monthly values of the Beaufort High and Southeastern High for the period 2000–2014 from NARR, including the standard deviations.

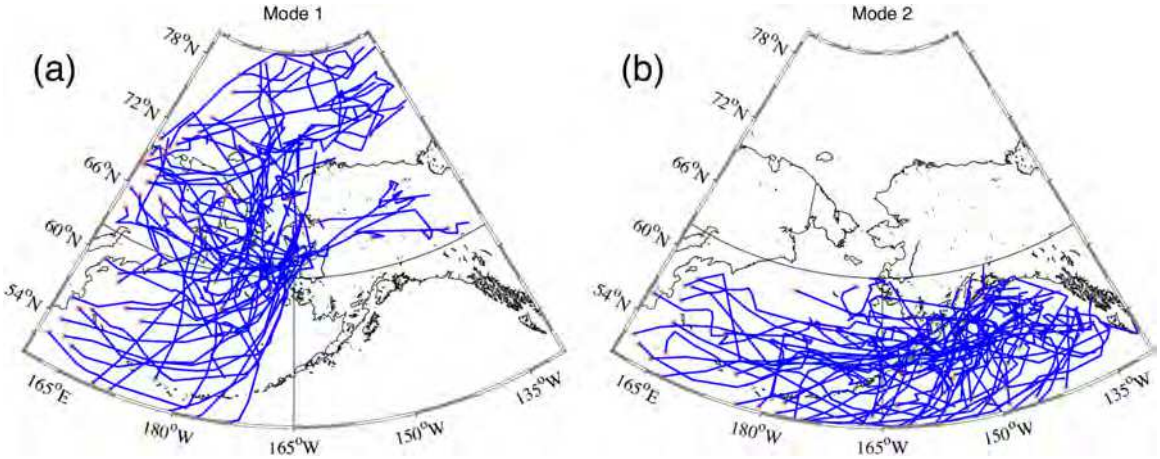

Fig. 14. Two dominant modes of storm tracks during the study period. (a) mode 1; (b) mode 2. The red asterisks denote where the storm was first identified in the study domain, and the blue lines are the tracks. The three sub-regions discussed in the text are marked by black lines. (For interpretation of the references to color in this figure legend, the reader is referred to the web version of this article.)

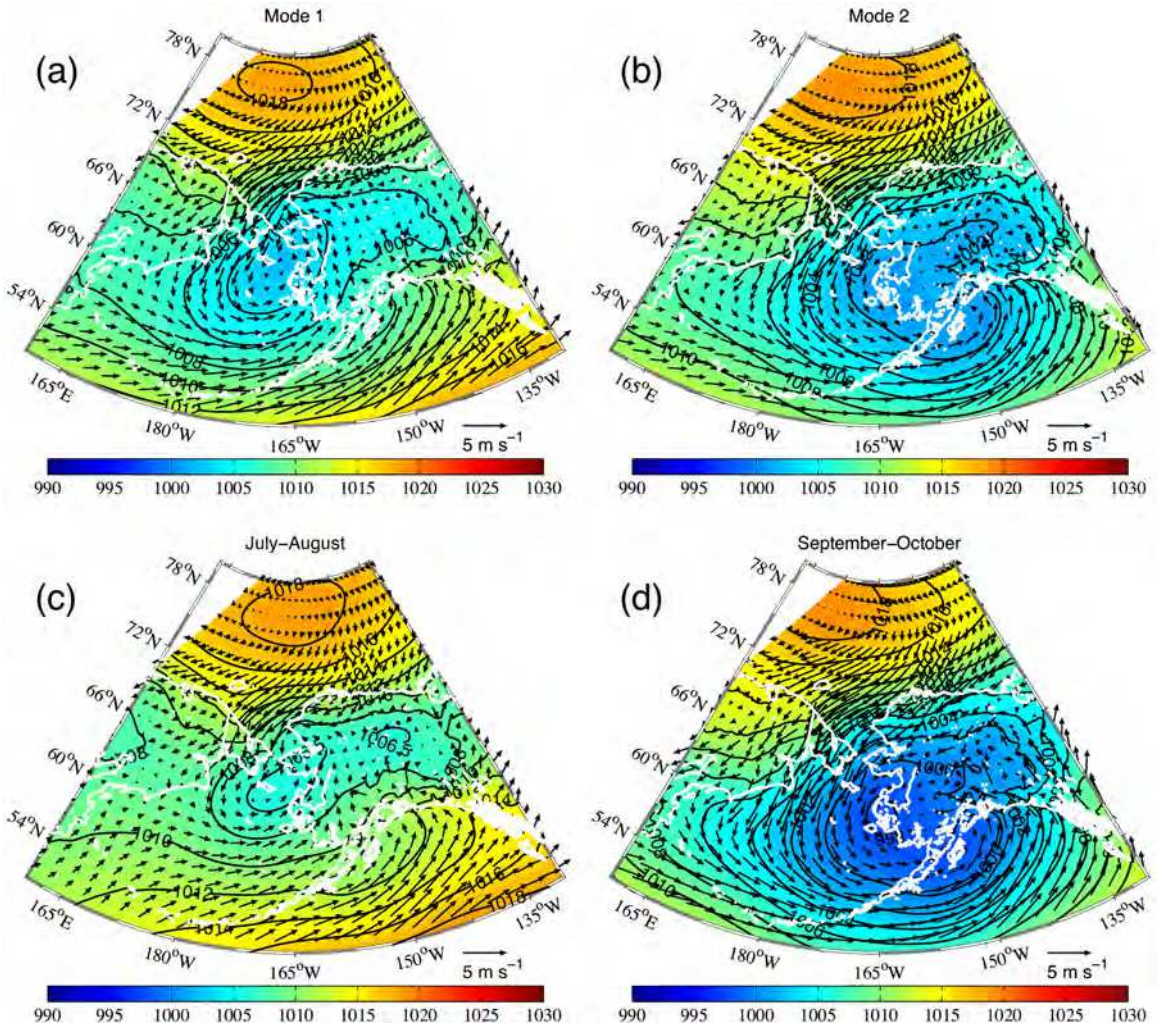

Fig. 16. (a) Composite SLP and 10 m wind from NARR during upwelling periods of mode 1 storms. (b) same as (a) for mode 2 storms. (c) Composite SLP and 10 m wind from NARR for all upwelling periods in July–August. (d) same as (c) for September–October.

the Beaufort High serves as a block and accordingly storms tend to travel eastwards. Both scenarios appear to be equally effective for driving upwelling in Barrow Canyon.

As the DBO program goes forward, and more sections are added to the timeseries, this will allow us to further refine the seasonal patterns identified here, and give us the opportunity to investigate the interannual variability of the water masses and wind-forced conditions in Barrow Canyon.

Acknowledgements

The authors are indebted to the officers and crew of the research vessels listed in Table 1 and to the many technicians who helped collect and process the data used in the study. We thank the anonymous reviewers and the guest editor, all of whom provided valuable input to the paper. Funding for the US component of DBO was provided by the National Science Foundation under grants ARC-1203906, ARC-1204044, ARC-1204082, PLR-1023331.

References

Aagaard, K., Roach, A.T., 1990. Arctic ocean-shelf exchange: measurements in Barrow Canyon. J. Geophys. Res. 95, 18,163–18,175.

Bourke, R.H., Paquette, R.G., 1976. Atlantic water on the Chukchi shelf. Geophys. Res. Lett. 3, 629–632.

Brugler, E.T., 2013. Interannual Variability of the Pacific Water Boundary Current in the BeaufortSea. Master's thesis, Massachusetts Institute of Technology and Woods Hole OceanographicInstitution, Cambridge/Woods Hole, WA. 120 pp.

Brugler, E.T., Pickart, R.S., Moore, G.W.K., Roberts, S., Weingartner, T.J., Statscewich, H., 2014. Seasonal to interannual variability of the Pacific water boundary current in the Beaufort Sea. Prog. Oceanogr. 127, 1–20.

Codispoti, L.A., Flagg, C., Kelly, V., Swift, J.H., 2005. Hydrographic conditions during the 2002 SBI process experiments. Deep Sea Res. II 52, 3199–3226.

Cooper, L., Frey, K., Logvinova, C., Biasatti, D., Grebmeier, J., 2016. Variations in the proportions of melted sea ice and runoff in surface waters of the Chukchi Sea: a retrospective analysis, 1990–2012, and analysis of the implications of melted sea ice in an under-ice bloom. Deep Sea Res. II 130, 6–13.

Corlett, W., Pickart, R.S., 2017. The chukchi slope current. Prog. Oceanogr. 153, 50–56.

Danielson, S., Eisner, L., Ladd, C., Mordy, C., Sousa, L., Weingartner, T., 2017. A comparison between late summer 2012 and 2013 water masses, macronutrients, and phytoplankton standing crops in the northern Bering and Chukchi Seas. Deep Sea Res. II 135, 7–26.

D'Asaro, E., 1988. Generation of submesoscale vortices: a new mechanism. J. Geophys. Res. 93, 6685–6693.

Gong, D., Pickart, R.S., 2015. Summertime circulation in the eastern Chukchi Sea. Deep Sea Res. II 118, 18–31.

Gong, D., Pickart, R.S., 2016. Early summer water mass transformation in the eastern Chukchi Sea. Deep Sea Res. II 130, 43–55.

Gonsior, M., Luek, J., Schmitt-Kopplin, P., Grebmeier, J., Cooper, L., 2017. Optical properties and molecular diversity of dissolved organic matter in the Bering Strait and Chukchi Sea. Deep Sea Res. II. https://doi.org/10.1016/j.dsr2.2017.01.003.

Grebmeier, J., Moore, S., Overland, J., Frey, K., Gradinger, R., 2010. Biological response to recent Pacific Arctic sea ice retreats. EOS, Trans. Am. Geophys. Union 91, 161–162.

Hill, V., Cota, G., 2005. Spatial patterns of primary production on the shelf, slope and basin of the western Arctic in 2002. Deep Sea Res. II 52, 335–3344.

Hill, V., Cota, G., Stockwell, D., 2005. Spring and summer phytoplankton communities in the Chukchi and eastern Beaufort Seas. Deep Sea Res. II 52, 3369–3385.

Huyer, A., Sobey, E., Smith, R., 1979. The spring transition in currents over the oregon

continental shelf. J. Geophys. Res. 84, 6995–7011.
Itoh, M., Nishino, S., Kawaguchi, Y., Kikuchi, T., 2013. Barrow Canyon volume, heat, and freshwater fluxes revealed by long-term mooring observations between 2000 and 2008. J. Geophys. Res. 118, 1–17.
Itoh, M., Pickart, R.S., Kikuchi, T., Fukamachi, Y., Ohshima, K.I., Simizu, D., Arrigo, K.R., Vagle, S., He, J., Ashjian, C., Mathis, J.T., Nishino, S., Nobre, C., 2015. Water properties, heat and volume fluxes of Pacific water in Barrow Canyon during summer 2010. Deep Sea Res. I 102, 43–54.
Itoh, M., Shimada, K., Kamoshida, T., McLaughlin, F., Carmack, E., Nishino, S., 2012. Inter-annual variability of Pacific winter water inflow through Barrow Canyon from 2000 to 2006. J. Oceanogr. 68, 575–592.
Ladd, C., Mordy, C.W., Salo, S.A., Stabeno, P.J., 2016. Winter water properties and the Chukchi polynya. J. Geophys. Res. 121, 5516–5534.
Li, M., Pickart, R.S., Spall, M.A., Weingartner, T.J., Lin, P., Moore, G., Qi, Y., 2019. Circulation of the Chukchi Sea shelfbreak and slope from moored timeseries. Prog. Oceanogr. https://doi.org/10.1016/j.pocean.2019.01.002.
Lin, P., Pickart, R., Stafford, K., Moore, G., Torres, D., Bahr, F., Hu, J., 2016. Seasonal variation of the Beaufort shelfbreak jet and its relationship to Arctic cetecean occurrence. J. Geophys. Res. 121. https://doi.org/10.1002/2016JC011890.
Lowry, K., Pickart, R., Mills, M., Brown, Z., van Dijken, G., Bates, N., Arrigo, K., 2015. Influence of winter water on phytoplankton blooms in the Chukchi Sea. Deep Sea Res. II 118, 53–72.
Mathis, J.T., Pickart, R.S., Hansell, D.A., Kadko, D., Bates, N.R., 2007. Eddy transport of organic carbon and nutrients from the Chukchi shelf into the deep Arctic basin. J. Geophys. Res. 112, C05011. https://doi.org/10.1029/2006JC003899.
Mesinger, F., DiMego, G., Kalnay, E., Mitchell, K., Shafran, P.C., Ebisuzaki, W., Jovic, D., Woollen, J., Rogers, E., Berbery, E.H., 2006. North American regional reanalysis. Bull. Am. Meteorol. Soc. 87 (3), 343–360.
Mountain, D.G., Coachman, L.K., Aagaard, K., 1976. On the flow through Barrow Canyon. J. Phys. Oceanogr. 6, 461–470.
Muench, R.D., Schumacher, J.D., Salo, S.A., 1988. Winter currents and hydrographic conditions on the northern central Bering Sea shelf. J. Geophys. Res. 93, 516–526.
Nikolopoulos, A., Pickart, R.S., Fratantoni, P.S., Shimada, K., Torres, D.J., Jones, E.P., 2009. The western arctic boundary current at 152° W: structure, variability, and transport. Deep Sea Res. II 56, 1164–1181.
Okkonen, S., Ashjian, C., Campbell, R., Maslowski, W., Clement-Kinney, J., Potter, R., 2009. Intrusion of warm Bering/Chukchi waters onto the shelf in the western Beaufort Sea. J. Geophys. Res. 114. https://doi.org/10.1029/2008JC004870.
Pacini, A., Pickart, R., Moore, G., Vage, K., 2016. Hydrographic structure and modification of Pacific winter water on the Chukchi Sea shelf in late spring. Eos Trans. AGU (AGU, abstract H14B-1406).
Pickart, R., Moore, G., Mao, C., Bahr, F., Nobre, C., Weingartner, T., 2016. Circulation of winter water on the Chukchi shelf in early summer. Deep Sea Res. II 130, 56–75.
Pickart, R., Schulze, L.M., Moore, G.W.K., Charette, M.A., Arrigo, K.R., van Dijken, G., Danielson, S.L., 2013. Long-term trends of upwelling and impacts on primary productivity in the Beaufort Sea. Deep Sea Res. I 79, 106–121.
Pickart, R.S., Moore, G.W.K., Macdonald, A.M., Renfrew, I.A., Walsh, J.E., Kessler, W.S., 2009a. Seasonal evolution of Aleutian low-pressure systems: implications for the North Pacific sub-polar circulation. J. Phys. Oceanogr. 39, 1316–1339.
Pickart, R.S., Moore, G.W.K., Torres, D.J., Fratantoni, P.S., Goldsmith, R.A., Yang, J., 2009b. Upwelling on the continental slope of the Alaskan Beaufort Sea: storms, ice, and oceanographic response. J. Geophys. Res. 114https://doi.org/10.1029/2208JC005009. (C00A13).
Pickart, R.S., Pratt, L.J., Torres, D.J., Whitledge, T.E., Proshutinsky, A.Y., Aagaard, K., Agnew, T.A., Moore, G.W.K., Dail, H.J., 2010. Evolution and dynamics of the flow through Herald Canyon in the western Chukchi Sea. Deep Sea Res. II 57, 5–26.
Pickart, R.S., Spall, M.A., Moore, G.W.K., Weingartner, T.J., Woodgate, R.A., Aagaard, K., Shimada, K., 2011. Upwelling in the Alaskan Beaufort Sea: atmospheric forcing and local versus non-local response. Prog. Oceanogr. 88, 78–100. https://doi.org/10.1016/j.pocean.2010.11.005.
Pickart, R.S., Stossmeister, G., 2008. Outflow of Pacific water from the Chukchi sea to the Arctic Ocean. Chin. J. Polar Oceanogr. 10, 135–148.
Pickart, R.S., Torres, D.J., Fratantoni, P.S., 2005. The east Greenland spill jet. J. Phys. Oceanogr. 35, 1037–1053.
Pisareva, M., Pickart, R., Spall, M., Nobre, C., Torres, D., Moore, G., 2015. Flow of pacific water in the western Chukchi Sea: results from the 2009 RUSALCA expedition. Deep Sea Res. I 105, 53–73.
Pisareva, M., Pickart, R., Fratantoni, P., Weingartner, T., 2019. On the nature of wind-forced upwelling in Barrow Canyon. Deep Sea Res. II 162, 63–78. https://doi.org/10.1016/j.dsr2.2019.02.002.
Schulze, L.M., Pickart, R.S., 2012. Seasonal variation of upwelling in the Alaskan Beaufort Sea: impact of sea ice cover. J. Geophys. Res. 117 (C06022). https://doi.org/10.1029/2012jc007985.
Shimada, K., Carmack, E., Hatakeyama, K., Takizawa, T., 2001. Varieties of shallow temperature maximum waters in the western Canadian Basin of the Arctic Ocean. Geophys. Res. Lett. 28, 3441–3444.
Shroyer, E., Pickart, R., 2019. Pathways, timing, and evolution of Pacific winter water through Barrow Canyon. Deep Sea Res. II.
Shroyer, E., Pleuddemann, A., 2012. Wind-driven modification of the Alaska coastal current. J. Geophys. Res. 117. https://doi.org/10.1029/2011JC007650.
Signorini, S., Munchow, A., Haidvogel, D., 1997. Flow dynamics of a wide Arctic canyon. J. Geophys. Res. 102, 18,661–18,680.
Spall, M.A., 2007. Circulation and water mass transformation in a model of the Chukchi Sea. J. Geophys. Res. 112, C05025. https://doi.org/10.1029/2005JC003364.
Spall, M.A., Pickart, R.S., Brugler, E.T., Moore, G., Thomas, L., Arrigo, K.R., 2014. Role of shelfbreak upwelling in the formation of a massive under-ice bloom in the Chukchi Sea. Deep Sea Res. II 105, 17–29.
Spall, M.A., Pickart, R.S., Li, M., Itoh, M., Lin, P., Kikuchi, T., Qi, Y., 2018. Transport of pacific water into the canada basin. J. Geophys. Res.
Våge, K., Pickart, R.S., Moore, G.W.K., Ribergaard, M.H., 2008. Winter mixed-layer development in the central Irminger Sea: the effect of strong, intermittent wind events. J. Phys. Oceanogr. 38, 541–565.
von Appen, W.-J., Pickart, R.S., 2012. Two configurations of the western Arctic shelfbreak current in summer. J. Phys. Oceanogr. 42, 329–351.
Weingartner, T.J., Aagaard, K., Woodgate, R., Danielson, S., Sasaki, Y., Cavalieri, D., 2005. Circulation on the north central Chukchi Sea shelf. Deep Sea Res. II 52, 3150–3174.
Weingartner, T.J., Cavalieri, D.J., Aagaard, K., Sasaki, Y., 1998. Circulation, dense water formation, and outflow on the northeast chukchi shelf. J. Geophys. Res. 103, 7647–7661.
Weingartner, T.J., Dobbins, E., Danielson, S., Winsor, P., Potter, R., Statscewich, H., 2013. Hydrographic variability over the northeastern Chukchi Sea shelf in summer-fall 2008–2010. Cont. Shelf Res. 67, 5–22.
Weingartner, T.J., Potter, R.A., Stoudt, C.A., Dobbins, E.L., Statscewich, H., Winsor, P.R., Mudge, T.D., Borg, K., 2017. Transport and thermohaline variability in Barrow Canyon on the northeastern Chukchi Sea shelf. J. Geophys. Res. 122. https://doi.org/10.1002/2016JC012636.
Winsor, P., Chapman, D., 2004. Pathways of pacific water across the Chukchi Sea: a numerial model study. J. Geophys. Res. 109. https://doi.org/10.1029/2003JC001962.
Woodgate, R.A., Aagaard, K., Weingartner, T.J., 2005. Monthly temperature, salinity, and transport variability of the Bering Strait throughflow. Geophys. Res. Lett. 32, L04601. https://doi.org/10.1029/2004GL021880.
Woodgate, R.A., Stafford, K., Prahl, F., 2015. A synthesis of year-round interdisciplinary mooring measurements in the Bering Strait (1990–2014) and the RUSALCA years (2004–2011). Oceanography 28, 46–67.